Cell Metabolism

Article

IL-22 resolves MASLD via enterocyte STAT3 restoration of diet-perturbed intestinal homeostasis

Graphical abstract

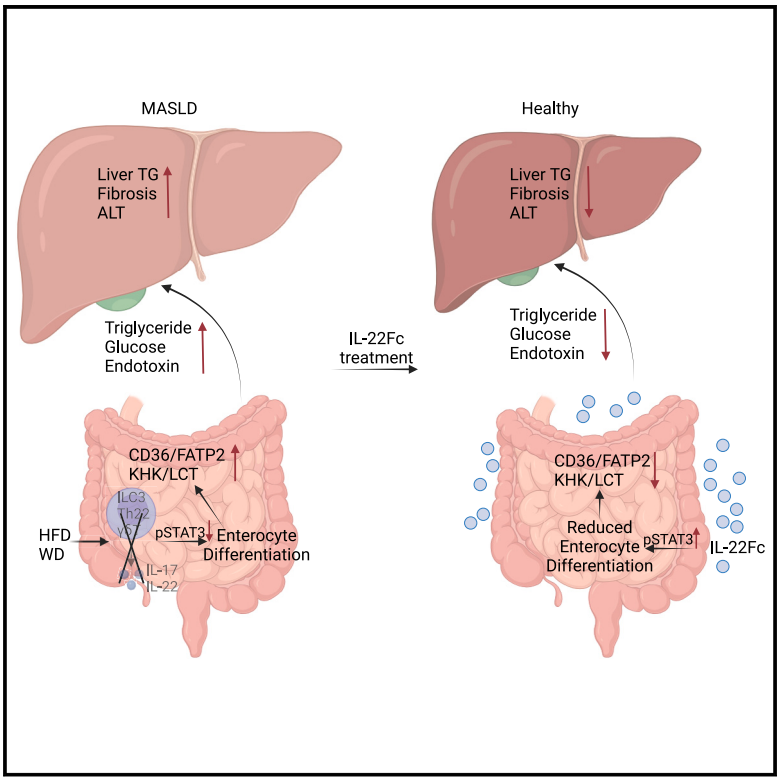

Authors

Peng Zhang, Junlai Liu, Allen Lee, ..., Bernd Schnabl, Pejman Soroosh, Michael Karin

Correspondence

karinoffice@ucsd.edu

In brief

Zhang et al. find that exogenously administered IL-22 resolved MASLD mainly by engaging its IEC receptor (IL-22Ra1), rather than hepatocytes, leading to STAT3-dependent restoration of diet-perturbed intestinal homeostasis.

Highlights

- Obesogenic diets inhibit intestinal IL-22 expression
- IL-22Fc resolves MASLD by engaging intestinal rather than hepatocytic IL-22Ra1
- IL-22Fc reduces fat absorption by reversing diet-induced enterocyte expansion
- IL-22Fc resolves MASLD by activating intestinal epithelial STAT3

Zhang et al., 2024, Cell Metabolism *36*, 2341–2354
October 1, 2024 Published by Elsevier Inc.
https://doi.org/10.1016/j.cmet.2024.08.012

CellPress

Cell Metabolism

CellPress
OPEN ACCESS

Article

IL-22 resolves MASLD via enterocyte STAT3 restoration of diet-perturbed intestinal homeostasis

Peng Zhang,[1,9] Junlai Liu,[1,9] Allen Lee,[1] Irene Tsaur,[1] Masafumi Ohira,[1] Vivian Duong,[1] Nicholas Vo,[1] Kosuke Watari,[1] Hua Su,[1] Ju Youn Kim,[1] Li Gu,[1] Mandy Zhu,[1] Shabnam Shalapour,[2] Mojgan Hosseini,[3] Gautam Bandyopadhyay,[4] Suling Zeng,[5] Cristina Llorente,[5] Haoqi Nina Zhao,[6] Santosh Lamichhane,[6,7] Siddharth Mohan,[6] Pieter C. Dorrestein,[6] Jerrold M. Olefsky,[4] Bernd Schnabl,[5] Pejman Soroosh,[8] and Michael Karin[1,10,*]

[1]Laboratory of Gene Regulation and Signal Transduction, Departments of Pharmacology and Pathology, School of Medicine, University of California, San Diego, La Jolla, CA 92093, USA
[2]Department of Cancer Biology, The University of Texas MD Anderson Cancer Center, Houston, TX, USA
[3]Department of Pathology, University of California, San Diego, San Diego, CA, USA
[4]Division of Endocrinology & Metabolism, University of California, San Diego, San Diego, CA, USA
[5]Department of Medicine, University of California, San Diego, San Diego, CA, USA
[6]Skaggs School of Pharmacy and Pharmaceutical Sciences, University of California, San Diego, San Diego, CA, USA
[7]Turku Bioscience Centre, University of Turku and Åbo Akademi University, 20520 Turku, Finland
[8]Janssen Research & Development, San Diego, CA 92121, USA
[9]These authors contributed equally
[10]Lead contact
*Correspondence: karinoffice@ucsd.edu
https://doi.org/10.1016/j.cmet.2024.08.012

SUMMARY

The exponential rise in metabolic dysfunction-associated steatotic liver disease (MASLD) parallels the ever-increasing consumption of energy-dense diets, underscoring the need for effective MASLD-resolving drugs. MASLD pathogenesis is linked to obesity, diabetes, "gut-liver axis" alterations, and defective interleukin-22 (IL-22) signaling. Although barrier-protective IL-22 blunts diet-induced metabolic alterations, inhibits lipid intake, and reverses microbial dysbiosis, obesogenic diets rapidly suppress its production by small intestine-localized innate lymphocytes. This results in STAT3 inhibition in intestinal epithelial cells (IECs) and expansion of the absorptive enterocyte compartment. These MASLD-sustaining aberrations were reversed by administration of recombinant IL-22, which resolved hepatosteatosis, inflammation, fibrosis, and insulin resistance. Exogenous IL-22 exerted its therapeutic effects through its IEC receptor, rather than hepatocytes, activating STAT3 and inhibiting WNT-β-catenin signaling to shrink the absorptive enterocyte compartment. By reversing diet-reinforced macronutrient absorption, the main source of liver lipids, IL-22 signaling restoration represents a potentially effective interception of dietary obesity and MASLD.

INTRODUCTION

Metabolic dysfunction-associated steatotic liver disease (MASLD) incidence has increased dramatically in the past 20–30 years, paralleling the exponential rise in dietary sugar and fat intake, making it one of the most common metabolic disorders.[1] MASLD is associated with lipotoxicity, insulin resistance, type 2 diabetes (T2D), metabolic activation of liver-stressing inflammatory and immune pathways, and microbial dysbiosis[2,3] and is a common Crohn's disease (CD) comorbidity.[4] The "gut-liver axis," which delivers luminal microbial metabolites and inflammatory mediators to the liver via the portal vein, has been proposed to be a key player in MASLD pathogenesis,[5] along with behavioral and dietary factors, including excessive consumption of energy-dense and ultra-processed foods.[2,6] Despite extensive efforts, only one MASLD-resolving drug has been clinically approved,[7] in addition to GLP1 receptor agonists, which resolve hepatosteatosis but not liver fibrosis.[8,9]

Interleukin-22 (IL-22) is a barrier-protective, antimicrobial cytokine produced by innate lymphocytes and Th17/22 cells,[10] whose signaling to intestinal epithelial cells (IECs) is inhibited by barrier-disruptive fructose- and fat-rich diets.[11] Endogenous IL-22 was suggested to prevent diet-induced metabolic disorders and inhibit lipid metabolism while shaping the gut microbiota.[12] Recombinant IL-22Fc fusion protein ameliorates T2D, MASLD, and related metabolic diseases in animal models[13] and is being assessed in phase II dose-escalation safety and efficacy studies in alcoholic hepatitis,[14] although its mechanism of action is not clear. As IL-22Fc is protective in models of acute hepatitis and high-fat diet (HFD)-induced hepatosteatosis,

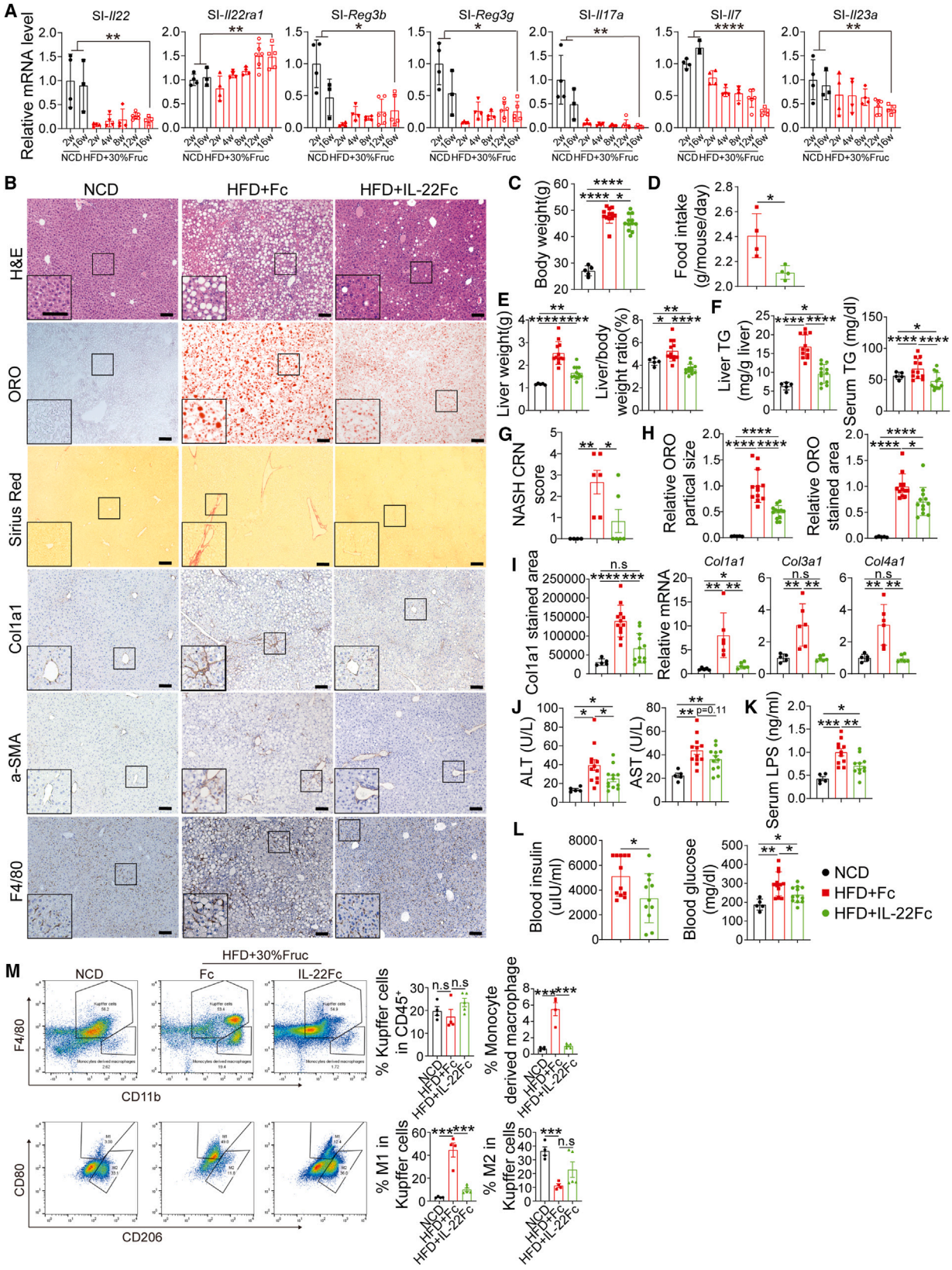

(legend on next page)

where it reduced lipogenic enzyme expression,[15–17] it was surmised to directly affect hepatocytes. However, IL-22 also reinforces the intestinal epithelial barrier and normalizes dysbiosis,[10] effects that could also contribute to the resolution of hepatosteatosis and metabolic dysfunction-associated steatohepatitis (MASH). Having found that an MASH-inducing high-fructose diet (HFrD) suppresses colonic IL-22 signaling,[11] we used additional diet-induced MASLD models and conditional ablations of the IL-22 receptor a1 subunit (IL-22Ra1) in hepatocytes or IECs to further investigate the dietary effects on IL-22 signaling and determine where and how IL-22Fc exerts its therapeutic activity. Here, we describe a vicious cycle in which prolonged intake of energy-dense diets suppresses IL-22 expression in small intestine (SI) innate lymphoid type 3 cells (ILC3s) and alters IEC differentiation and maturation to increase fat and sugar uptake, effects that are reversed by exogenous IL-22Fc to result in MASLD resolution.

RESULTS

Diet-induced MASLD is resolved by exogenous IL-22

We used two diet-induced MASLD models that, due to lower fructose content than our previously used HFrD model,[11] are more similar to energy-dense human diets. The first model employed an HFD in which 60% of the calories are provided by fat, 25% by carbohydrates, and 15% by protein, supplemented with a 30% fructose drink. The second model was based on a Western diet (WD) in which 40.1% of the calories are derived from fat, 44.4% from carbohydrates (34% sucrose by weight), and 15.5% from protein, as well as 0.2% cholesterol, which was also supplemented with a 30% fructose drink. HFD + fructose drink and, to a lesser extent, WD + fructose strongly and rapidly suppressed SI mRNA and protein expression of IL-22, IL-17a, Reg3β, and Reg3γ, as well as STAT3 phosphorylation, and more modestly reduced *Il23* and *Il7* mRNAs, whose products expand IL-17- and IL-22-producing cells[18] (Figures 1A and S1A–S1D). To test whether exogenous IL-22 can resolve diet-induced MASLD, mice that were kept for 12 weeks on either diet and displayed hepatosteatosis accompanied by different degrees of inflammation and fibrosis were intraperitoneally (i.p.) injected with 10 μg IL-22Fc or Fc isotype control every 3 days for a total of 4 weeks, during which the obesogenic diets were continued (Figure S1E). At the end of these regimens, the mice were culled and their livers were analyzed. Compared with normal chow diet (NCD)-fed mice, mice maintained on either obesogenic diet and that had received Fc control showed pronounced hepatosteatosis, accompanied by mild to extensive fibrosis, and modest liver damage, marked by elevated circulating amounts of the liver enzymes ALT and AST (Figures 1B–1J and S1F–S1K). IL-22Fc treatment blunted body weight (BW) gain in both models and reduced food intake (Figures 1C, 1D, S1F, and S1G); resolved hepatosteatosis, hepatic stellate cell (HSC) activation/expansion, liver fibrosis, and fibrogenic gene expression; and markedly reduced endotoxemia and insulin resistance in the HFD + 30% fructose drink model (Figures 1B–1L). IL-22Fc also resolved hepatosteatosis and inhibited liver damage, hyperlipidemia, and insulin resistance in mice kept on a WD + 30% fructose drink (Figures S1F–S1N). In addition, IL-22Fc treatment reduced M1-type Kupffer cells (KCs) and monocyte-derived macrophages in both models but had no effect on total KC number (Figures 1M and S1O). Administration of either Fc control or IL-22Fc had insignificant effects on BW, liver weight, and liver histology in NCD-fed BL6 mice (Figures S1P–S1R).

MASLD resolution depends on IL-22 signaling in IECs rather than hepatocytes

Given the key role of the gut-liver axis in MASLD/MASH development,[11] we examined whether IL-22Fc exerts its beneficial effects in hepatocytes or IECs. We used *Il22ra1*$^{f/f}$ mice,[19] crossed with either *Albumin*^{Cre} (*Alb*^{Cre}/*Il22ra1*$^{f/f}$) or *Villin*^{Cre} (*Villin*^{Cre}/*Il22ra1*$^{f/f}$) mice, to ablate IL-22Ra1 in either hepatocytes (*Il22ra1*$^{\Delta Hep}$) or IECs (*Il22ra1*$^{\Delta IEC}$). Either ablation selectively blocked IL-22Fc-induced STAT3 phosphorylation as well as *Il22ra1* mRNA expression in the respective cell type, while *Il22ra1*$^{\Delta Hep}$ mice did not show *Lcn2* mRNA induction in the liver and *Il22ra1*$^{\Delta IEC}$ mice did not exhibit *Reg3g* mRNA induction in the SI (Figures S2A–S2E). Curiously, only IEC-specific, but not hepatocyte-specific, IL-22Ra1 ablation blocked IL-22Fc-induced MASLD resolution in HFD + 30%-fructose-fed mice (Figures 2A–2D). *Il22ra1*$^{\Delta IEC}$ mice also did not respond to IL-22Fc with reduced body and liver weights, lower liver

Figure 1. Exogenous IL-22 resolves diet-induced hepatosteatosis and fibrosis

(A) Quantitative real-time PCR of the indicated SI mRNAs collected from C57BL/6 mice at the indicated times after initiation of NCD or HFD + 30% fructose drink feeding (NCD 2 weeks, $n = 4$; NCD 16 weeks, $n = 3$; HFD 2 weeks, $n = 4$; HFD 4 weeks, $n = 4$; HFD 8 weeks, $n = 4$; HFD 12 weeks, $n = 6$; HFD 16 weeks, $n = 5$).

(B–M) C57BL/6 mice were placed on NCD ($n = 5$) or HFD + 30% fructose water for 16 weeks and treated with Fc isotype control ($n = 12$) or IL-22Fc ($n = 12$) (10 μg/dose/3 days) for the last 4 weeks.

(B) Representative H&E, oil red O (ORO), and Sirius red staining and Col1a1, αSMA, and F4/80 IHC of liver sections. Scale bars, 100 and 200 μm (inset).

(C) Body weight (BW).

(D) Food intake.

(E) Liver weight and liver/body weight ratio.

(F) Liver and serum TG.

(G) NASH CRN scores.

(H) Quantification of ORO staining in (B).

(I) Quantification of Col1a1 staining in (B) and relative *Col1a1*, *Col3a1*, and *Col4a1* mRNA amounts.

(J) Serum ALT and AST concentrations.

(K) Serum lipopolysaccharide (LPS).

(L) Blood insulin and glucose.

(M) Gating strategy and percentage of M1 (CD80$^+$) and M2 (CD206$^+$) Kupffer cells (CD45$^+$LIN$^-$F4/80$^+$CD11b^{int}) and monocyte-derived macrophages (CD45^{+-}LIN$^-$F4/80$^-$CD11b^{Hi}) from NCD- ($n = 4$) or HFD-fed mice treated with Fc ($n = 4$) or IL-22Fc ($n = 5$).

Data are presented as mean ± SEM. $^*p < 0.05$, $^{**}p < 0.01$, $^{****}p < 0.0001$ (unpaired two-tailed t test).

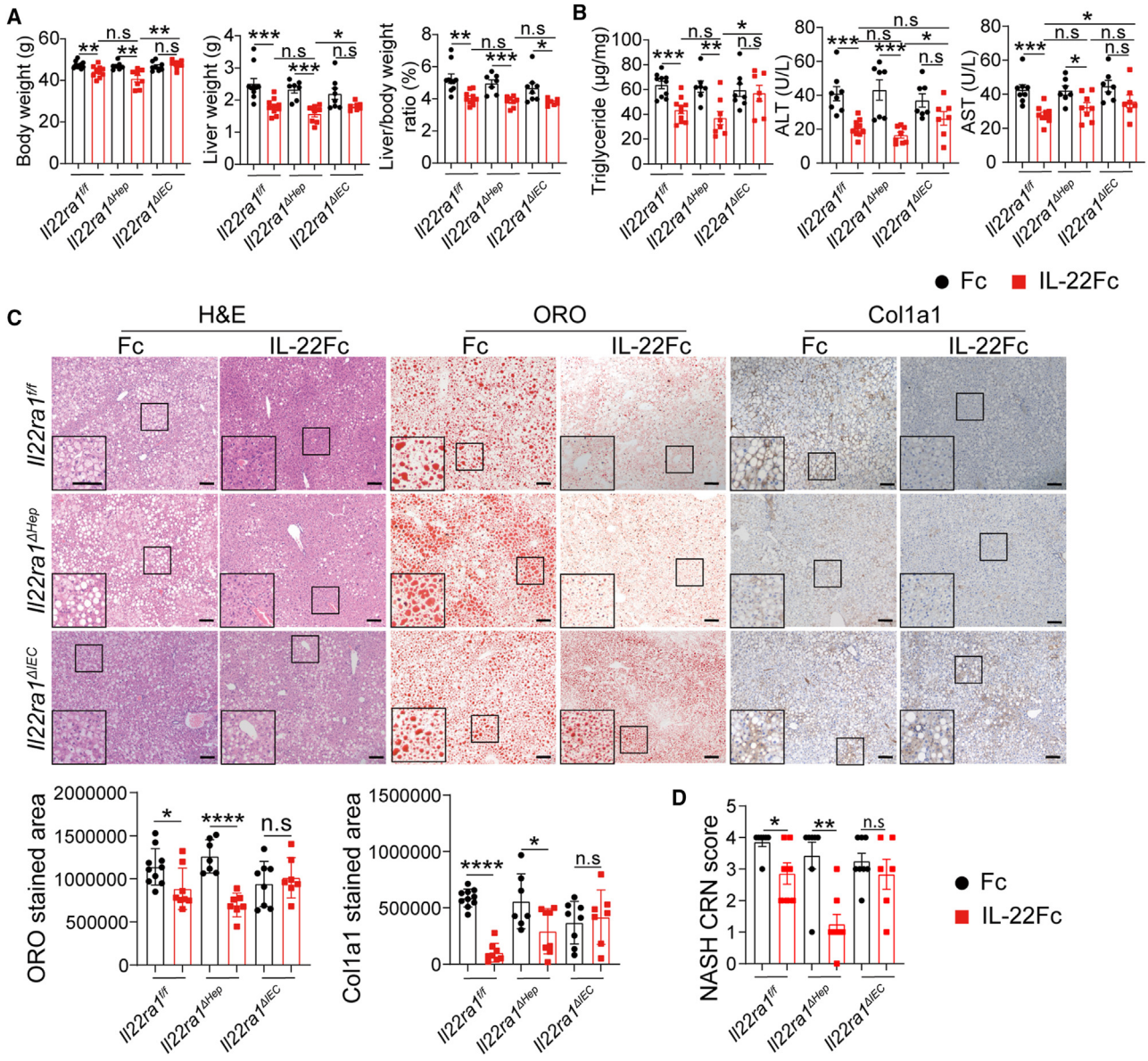

Figure 2. IL-22Fc signals in IECs to resolve MASLD

Il22ra1$^{f/f}$ (Fc, $n = 10$; IL-22Fc, $n = 10$), *Il22ra1*$^{\Delta Hep}$ (Fc, $n = 7$; IL-22Fc, $n = 8$), and *Il22ra1*$^{\Delta IEC}$ (Fc, $n = 8$; IL-22Fc, $n = 7$) mice were placed on an HFD + 30% fructose water for 16 weeks and treated with Fc or IL-22Fc, as above.

(A) BW, liver weight, and liver/body weight ratio.

(B) Liver TG, serum ALT, and AST.

(C) Representative H&E, ORO, and Col1a1 IHC of liver sections and quantification. Scale bars, 100 and 200 μm (inset).

(D) NASH CRN scores of above mice.

Data are presented as mean ± SEM. n.s., not significant; *$p < 0.05$, **$p < 0.01$, ***$p < 0.001$ (unpaired two-tailed t test).

damage, and decreased collagen 1a1 (Col1a1) accumulation compared with Fc-treated mice, while hepatocyte-specific IL-22Ra1 ablation had little effect on any of these parameters. To validate the surprisingly nonessential role of hepatocyte IL-22Fc signaling, we used hepatocyte-specific *Stat3* knockout mice (*Alb*^{Cre}/*Stat3*$^{f/f}$, *Stat3*$^{\Delta Hep}$) kept on HFD + 30% fructose. Treatment of these mice with IL-22Fc still led to resolution of MASLD, along with reduced body and liver weights and inhibition of *Lcn2* mRNA induction (Figures S2F–S2M).

Given previous reports that IL-22Fc reduces hepatic gluconeogenesis, a hepatocyte-intrinsic process,[20] we tested its ability to signal in hepatocytes, using multi-lineage spheroids (MLSs) consisting of hepatocytes, HSCs, and macrophages/KC.[21] Incubation of MLS in "NASH medium," containing fatty acids, fructose, and endotoxin, upregulated genes encoding fibrogenic proteins, inflammatory cytokines, and lipogenic enzymes, an effect that was blocked by IL-22Fc, which induced β-oxidation genes (Figures S3A and S3B). MLS generated with *Il22ra1*$^{\Delta Hep}$

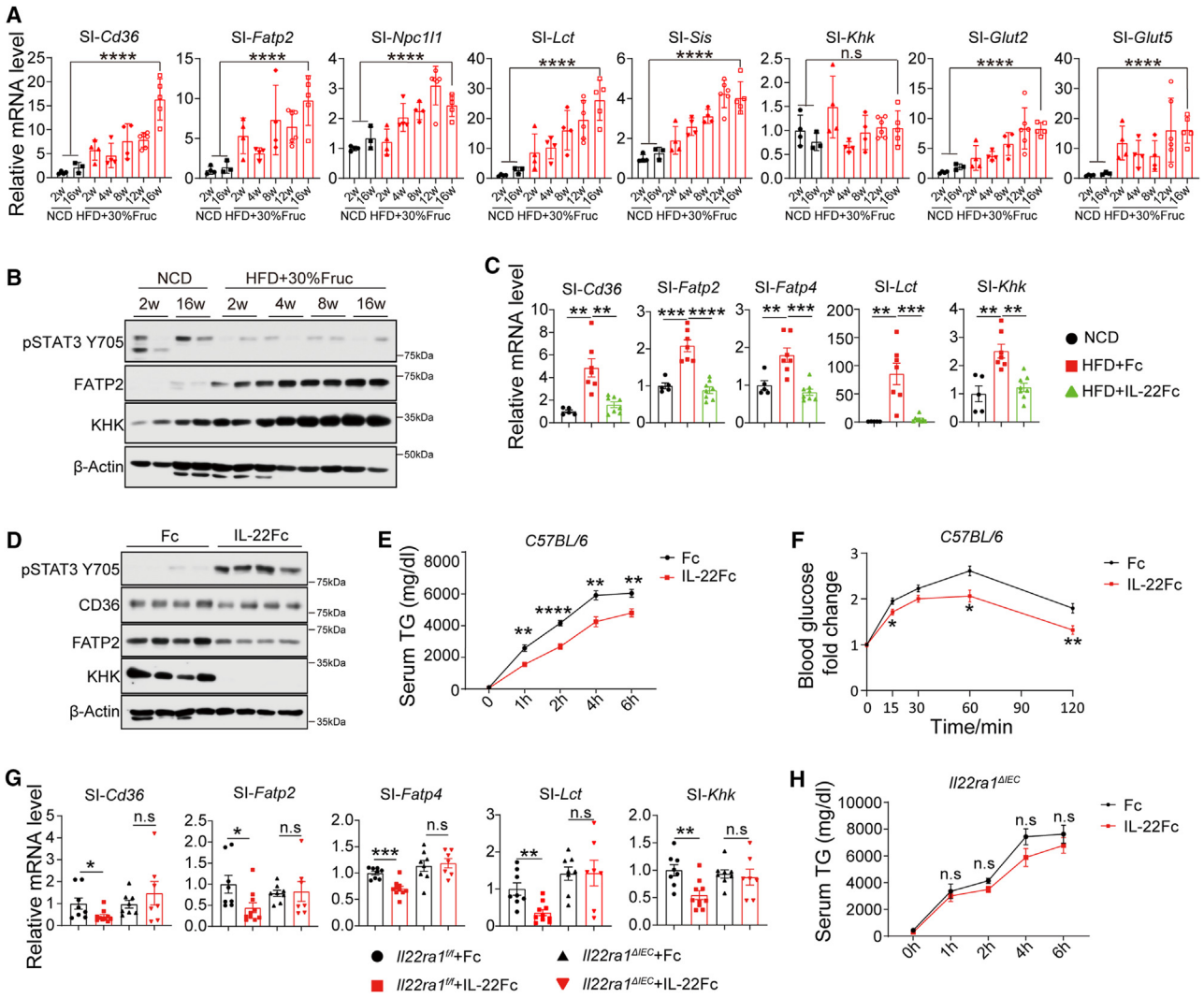

Figure 3. IL-22Fc signaling in IECs inhibits macronutrient uptake and metabolism

(A and B) Quantitative real-time PCR of indicated mRNAs (A) and immunoblot of indicated proteins (B) in SI of C57BL/6 mice at the indicated times after initiation of NCD or HFD + 30% fructose water feeding (NCD 2 weeks, $n = 4$; NCD 16 weeks, $n = 3$; HFD 2 weeks, $n = 4$; HFD 4 weeks, $n = 4$; HFD 8 weeks, $n = 4$; HFD 12 weeks, $n = 6$; HFD 16 weeks, $n = 5$).

(C) Relative mRNA amounts of indicated genes in the SI of NCD- ($n = 5$) or HFD + fructose-drink-fed mice treated with Fc ($n = 7$) or rIL-22Fc ($n = 8$), as above.

(D) IB analysis of SI proteins in above mice.

(E and H) Serum TGs after olive oil gavage of Fc- or IL-22Fc-treated C57BL/6 mice (E) or *Il22ra1*$^{\Delta IEC}$ mice (H) that were HFD fed for 2 weeks (E, Fc, $n = 7$; IL-22Fc, $n = 7$; H, Fc, $n = 5$; IL-22Fc, $n = 6$).

(F) Blood glucose after 20% lactose gavage of Fc- or IL-22Fc-treated C57BL/6 mice (Fc, $n = 5$; IL-22Fc, $n = 8$).

(G) Quantitative real-time PCR of indicated genes in SI of HFD + 30%-fructose-fed *Il22ra1*$^{f/f}$ and *Il22ra1*$^{\Delta IEC}$ mice treated with Fc or IL-22Fc, as above.

Data are presented as mean ± SEM. n.s., not significant; $^{*}p < 0.05$, $^{**}p < 0.01$, $^{***}p < 0.001$ (unpaired two-tailed t test).

hepatocytes reacted to NASH medium like wild-type MLS but no longer responded to IL-22Fc (Figures S3A and S3B). These results indicate that although IL-22 can certainly modify the expression of liver metabolism and fibrogenesis genes, these effects are irrelevant to the resolution of diet-induced MASLD, which depends on the gut-liver axis and IL-22 signaling in IECs. We therefore checked whether hepatocyte IL-22Ra1 signaling has a role in a different *in vivo* model of liver injury induced by ethanol, which acts directly on hepatocytes rather than being absorbed by SI IECs and delivered to the liver via the portal vein (Figure S3C). This time, hepatocyte-specific *Il22ra1* ablation blocked the protective effect of IL-22Fc (Figure S3D), while the IEC-specific ablation had no effect (Figure S3E). These results illustrate that IL-22 signaling in hepatocytes is of protective relevance as long as the corresponding challenge acts directly on hepatocytes and not via other cell types.

IL-22Fc can suppress macronutrient absorption independently of the microbiota

As lipid and sugar absorption, which sustain BW gain and hepatosteatosis, take place in the SI, we examined whether IL-22Fc

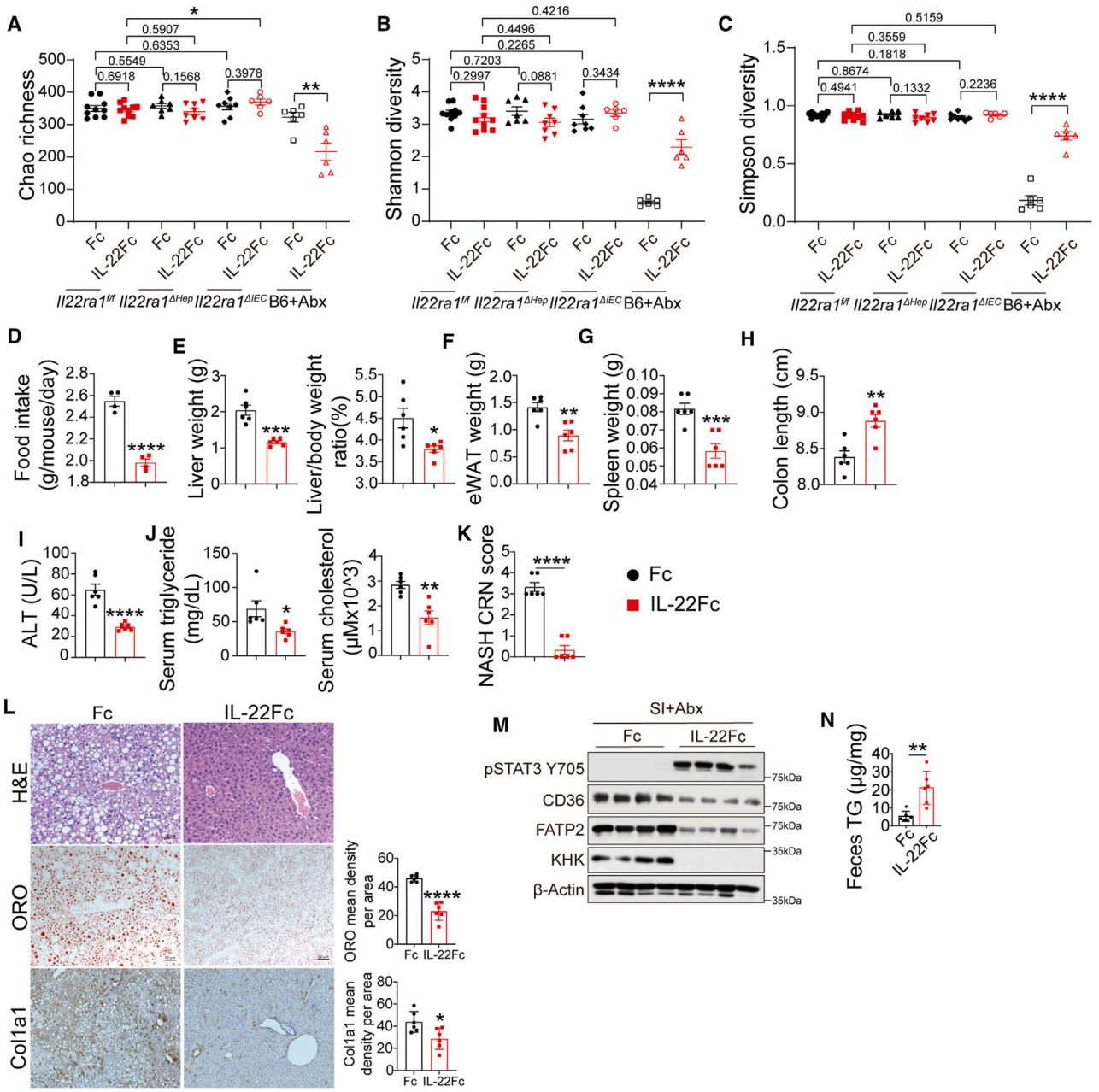

Figure 4. IL-22Fc resolves MASLD in microbiota-depleted mice

(A–C) The fecal microbiome of the indicated mice (*Il22ra1*$^{f/f}$ [Fc, $n = 10$; IL-22Fc, $n = 10$], *Il22ra1*$^{\Delta Hep}$ [Fc, $n = 7$; IL-22Fc, $n = 8$], *Il22ra1*$^{\Delta IEC}$ [Fc, $n = 8$; IL-22Fc, $n = 7$], and C57BL/6 + Abx [Fc, $n = 6$; IL-22Fc, $n = 6$]), which were HFD + fructose fed and treated with Fc or IL-22Fc, as above, was investigated by 16S sequencing.

(A) Chao richness.

(B) Shannon diversity.

(C) Simpson diversity.

(D–N) C57BL/6 mice were fed HFD + fructose for 16 weeks and treated with Abx for the last 5 weeks, followed by Fc ($n = 6$) or IL-22Fc ($n = 6$) treatments as above.

(D) Food intake.

(E) Liver weight and liver/body weight ratio.

(F) eWAT weight.

(G) Spleen weight.

(H) Colon length.

(I and J) Serum ALT (I), TG, and cholesterol (J).

(K) NASH CRN scores.

(legend continued on next page)

affected expression of SI proteins involved in macronutrient absorption and catabolism, some of which were reported to be modulated by endogenous IL-22 during short-term dietary challenges.[12,22,23] HFD + fructose feeding increased the mRNA and protein amounts of the lipid transporters CD36, FATP2, and FATP4; the sugar transporters Glut2 and Glut5; and the sugar mobilizing and metabolizing enzymes ketohexokinase (KHK) and lactase (LCT), along with inhibition of basal STAT3 phosphorylation (Figures 3A and 3B). These effects, which were also seen in WD + fructose-fed mice, were reversed by IL-22Fc (Figures 3C and S3F), which also inhibited their protein expression (Figure 3D). IL-22Fc also inhibited TG transport from the SI to the blood in mice given HFD for 1 week followed by olive oil gavage and reduced blood glucose in mice gavaged with a 20% lactose solution (Figures 3E and 3F), suggesting inhibition of lactose hydrolysis and uptake. Suppression of lipid transporters and TG uptake was dependent on IL-22Ra1 engagement in IECs (Figures 3G and 3H). Consistent with the inhibition of lipid absorption, steady-state metabolomic analysis revealed that IL-22Fc treatment reduced the hepatic amounts of storage lipids (TGs, diacylglycerols [DGs], and cholesterols), phosphotadylcholine (PC), phosphatidylethanolamine (PE), and arachidonoylithio-PC and reversed the MASLD-related increase in lyso-phosphatidylethanolamine (LPE)[24] in mice fed WD + fructose (Figure S4A). Curiously, the ratio of lyso-phosphatidylcholine (LPC) to LPE, which is reduced in MASLD,[24] was increased in the livers of IL-22Fc-treated mice, as were the amounts of hepatic retinoids, which were also reported to decrease in MASLD.[25] These results are consistent with the ability of retinoids to reduce hepatosteatosis.[26]

As expected,[27] IL-22Fc treatment reduced barrier permeability and increased the expression of tight junction protein (TJP) mRNAs in HFD + fructose-fed mice (Figures S4B and S4C). However, counter to the known ability of IL-22 to restore microbial homeostasis,[28] microbiome (16S) sequencing showed the rather modest effects of IL-22Fc on total fecal microbiome diversity in HFD + fructose-fed mice, although these effects were somewhat obscured by differences in microbiome composition between the 3 mouse strains (Figures 4A–4C, S4D, and S4E). To functionally examine the contribution of the intestinal microbiota to the therapeutic effects of IL-22Fc, mice were fed HFD + fructose drink for 16 weeks, followed by 5 weeks' treatment with an antibiotics cocktail (Abx), which markedly reduced (90%) fecal bacterial 16S RNA and serum endotoxin amounts (Figures S4F and S4G). After 1 week on Abx, the mice were given IL-22Fc or Fc for 4 weeks and analyzed. Abx treatment transiently reduced BW gain, which was eventually restored in Fc-treated mice, and further enhanced and sustained in IL-22Fc-treated mice, which, in addition to lower BW, showed a further decrease in fecal 16S RNA and serum endotoxin (Figures S4G and S4H). Notably, IL-22Fc treatment decreased food intake—as well as liver, eWAT, and spleen weights—while increasing colon length and suppressing hepatosteatosis, Col1a1 expression, liver damage, and serum lipids in Abx-treated HFD + fructose-fed mice (Figures 4D–4L, S4I, and S4J). IL-22Fc also continued to reduce SI CD36, FATP2, and KHK expression and increase fecal triglycerides (Figures 4M and 4N), an effect consistent with inhibition of lipid absorption. We conclude that, despite its well-established effect on microbial homeostasis, many of the therapeutic effects of IL-22Fc are retained in microbiota-depleted mice.

IL-22Fc reverses diet-induced expansion of mature absorptive enterocytes

Re-analysis of a previous single-cell RNA sequencing (scRNA-seq) study showed that HFD feeding altered the steady-state composition of the SI epithelium,[29] expanding the mature enterocyte and enterocyte progenitor compartments (Figure S5A). To determine the effect of IL-22Fc on the same subpopulations, we conducted an scRNA-seq study of SI IECs from mice fed HFD + fructose for 16 weeks and treated with Fc or IL-22Fc for the last 4 weeks. Intriguingly, IL-22Fc treatment had the opposite effect to continuous HFD + fructose feeding, minimizing the stem cell and mature enterocyte compartments and expanding transit-amplifying enterocyte progenitors (Figures 5A–5C). Moreover, IL-22Fc suppressed *Lct* and *Cd36* mRNA expression in mature enterocytes and increased gasdermin C2 (*Gsdmc2*) mRNA, a transit-amplifying cell marker, in enterocyte progenitors (Figure 5C), effects opposite to those of HFD feeding (Figure S5B). Gene Ontology (GO) and gene set enrichment analysis (GSEA) revealed that, opposite to HFD, IL-22Fc suppressed FA metabolism and transport genes (Figures 5D, 5E, and S5C). The effect of IL-22Fc on IEC homeostasis was confirmed by quantitative real-time PCR analysis of mature enterocytes, enterocyte progenitors, and intestinal stem cell markers and IHC of CD36 and sucrase isomaltase (SIS) (Figures S5D and S5E). IL-22Fc also decreased SOX9 protein expression in the stem cell compartment and increased crypt length (Figure S5E). Expansion of enterocyte progenitors expressing *Prom1* and *Prss2* mRNAs by IL-22Fc was dependent on IL-22Ra1 expression in IECs (Figure S5F).

STAT3 activation and Wnt-β-catenin-signaling inhibition mediate IL-22 action

We investigated how IL-22Fc restores IEC homeostasis. An HFD + fructose feeding markedly suppressed activating Y705 STAT3 phosphorylation in SI IECs, as well as degradation-inducing S33/37 and T41 β-catenin phosphorylation, while modestly increasing GSK3β S9 phosphorylation, which inhibits substrate binding, and strongly inducing CD36, FATP2, and KHK protein expression (Figure 6A). Consistent with the above and a previous report,[30] HFD + fructose feeding stimulated expression of β-catenin-responsive *Bmp4*, *Jag1*, *Lgr5*, *Lrp6*, and *Tcf1* mRNAs (Figure 6B). IL-22Fc treatment reversed these effects, decreasing GSK3β S9 phosphorylation and *Axin2*, *Wnt3*, *Lrp5*, and *Cd44* mRNAs, while enhancing degradative β-catenin phosphorylation and reducing its nuclear amounts (Figures 6C and 6D). Inhibition of β-catenin signaling was also

(L) Representative H&E, ORO, and Col1a1 IHC of liver sections and their quantification. Scale bar, 100 μm.
(M) IB analysis of indicated SI proteins.
(N) TG in feces from the indicated mice.
Data are presented as mean ± SEM. $^{*}p < 0.05$, $^{**}p < 0.01$, $^{***}p < 0.001$, $^{****}p < 0.0001$ (unpaired two-tailed t test).

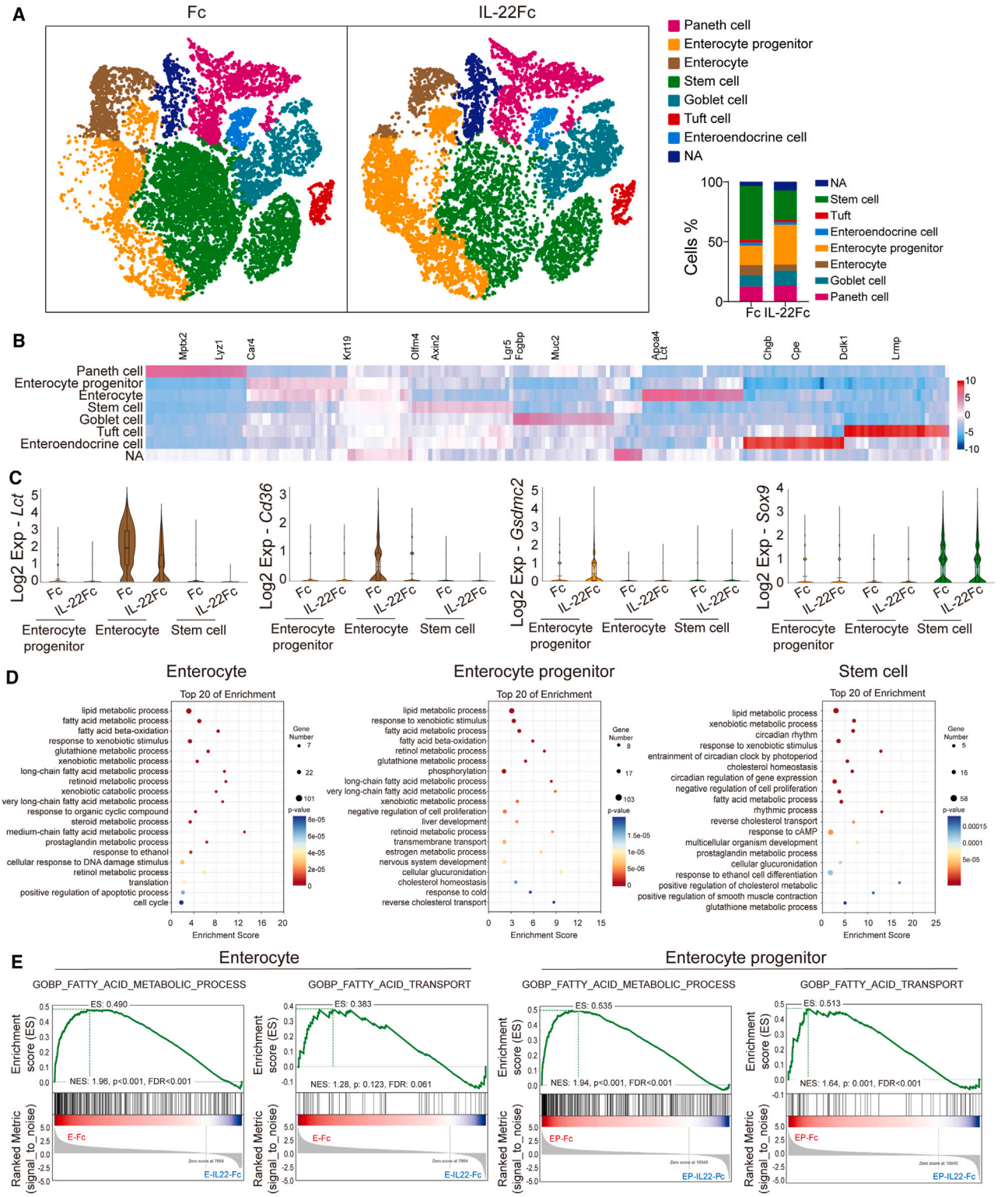

Figure 5. IL-22Fc restores diet-perturbed IEC homeostasis, reducing mature absorptive enterocytes and increasing enterocyte progenitors

The SI of C57BL/6 mice fed HFD + fructose and treated with Fc or IL-22Fc, as above, was isolated and single-cell suspensions of crypt epithelial cells were subjected to RNA sequencing.

(A) t-distributed stochastic neighbor embedding (t-SNE) plots depicting color-coded clustering of 17,213 and 14,660 single epithelial cells from Fc- and rIL-22Fc-treated mice, respectively (n = 2 mice per group), based on known marker genes. The bar graphs show frequencies of different epithelial subsets.

(legend continued on next page)

evident from the scRNA-seq data, which showed reduced SI β-catenin signature transcripts in the IL-22Fc-treated group (Figure 6E).

Given the inhibition of STAT3 activation by HFD + fructose and its stimulation by IL-22Fc, we interrogated its role as an IL-22 effector by ablating the *Stat3* gene in IECs.[31] *Stat3*$^{\Delta IEC}$ mice fed with HFD + fructose drink no longer responded to IL-22Fc with reduced food intake, body, and liver weights, and although IEC STAT3 ablation modestly increased liver damage, it prevented its reversal by IL-22Fc (Figures 7A and S6A–S6F). In *Stat3*$^{\Delta IEC}$ mice, IL-22Fc no longer decreased SI CD36 and SOX9 (Figure S6G). By contrast, STAT3 ablation in hepatocytes had no effect on the IL-22Fc-mediated suppression of intestinal CD36, FATP2, and KHK in HFD + fructose-fed mice and the induction of *Reg3b* and *Reg3g* mRNAs (Figures S6H and S6I). Consistent with its presumed role in suppression of lipid and sugar absorption and catabolism, IEC-specific STAT3 ablation markedly increased *Cd36*, *Fatp2*, *Lct*, and *Khk* SI mRNAs in NCD-fed mice and extinguished *Il22* mRNA while increasing *Il22ra1* mRNA (Figure 7B). The latter results suggested that inhibition of IEC STAT3 may account for the diet-induced suppression of *Il22* mRNA expression through a poorly understood communication between IECs and IL-22-producing cells.[32] Indeed, scRNA-seq analysis of SI CD45$^+$ cells from HFD + fructose-fed and IL-22Fc-treated mice showed that IL-22Fc signaling in IECs restored *Il22* mRNA in ILC3 cells, *Il17a* mRNA in Th17 cells, and *Il23a* mRNA in macrophages and dendritic cells (DCs) (Figures 7C and 7D). IL-22Fc treatment also altered the composition of SI CD45$^+$ cells, increasing the number of Th17 cells, DCs, and CD8$^+$ T cells and reducing the number of plasma cells, as well as reversing the HFD-induced reduction in IL-22$^+$ ILC3 cells (Figures 7C and 7E). Curiously, HFD + fructose feeding partially reduced *Cd36*, *Fatp2*, *Lct*, and *Khk* mRNAs in *Stat3*$^{\Delta IEC}$ mice, but IL-22Fc no longer modulated their expression (Figure 7B). STAT3 ablation also abrogated expression of *Lgr5*, *Olfm4*, and *Wnt3* mRNAs and partially decreased *Axin2* mRNA in NCD-fed mice (Figure 7B), suggesting that STAT3 activation is not the main cause of Wnt-β-catenin-signaling inhibition by IL-22Fc.

To further interrogate the role of IEC STAT3, we examined *Villin-gp130Act* mice (*gp130*$^{Act\text{-}IEC}$), which express a constitutively active variant of IL-6ST (gp130) in IECs,[33] which were HFD fed for 16 weeks (Figure S7A). Surprisingly, *gp130*$^{Act\text{-}IEC}$ mice were resistant to HFD-induced MASLD, although they consumed more HFD than WT mice (Figures S7B–S7I). Like IL-22Fc-treated mice, the SI of *gp130*^{Act} mice showed STAT3 and YAP1 activation while expressing lower amounts of CD36, FATP2, FATP4, and KHK (Figures S7J and S7K). Taken together, these data underscore the notion that intestinal STAT3 signaling is a key downstream mediator of IL-22Fc's ability to resolve MASLD.

DISCUSSION

The beneficial metabolic effects of exogenous IL-22 are well established,[13,34] supporting the clinical development of IL-22Fc fusion proteins for the treatment of MASLD and alcoholic hepatitis.[14] However, the cellular targets for the therapeutic effects of IL-22 and its mechanism of action remained largely unknown. Here, we show that, counter to previous expectations that IL-22's hepatoprotective effects are solely mediated via its hepatocyte receptor, the resolution of diet-induced mouse MASLD by IL-22Fc entirely depends on IL-22Ra1 engagement and STAT3 activation in IECs. These results underscore the previously described critical role of the intestinal mucosa and the gut-liver axis in MASLD/MASH pathogenesis[4,11,35] and the dependence of hepatosteatosis on dietary fat and sugar intake rather than hepatocyte-intrinsic *de novo* lipogenesis and defective β-oxidation.[36] Nonetheless, these results are model and insult specific. In the case of alcohol, which is readily absorbed in the stomach and SI without a need for specialized transporters and reaches the liver to cause hepatocyte injury and fat deposition, the protective effect of IL-22Fc does depend on engagement of its hepatocyte receptor. Moreover, *ex vivo* studies using MLSs as a model clearly demonstrate that exogenous IL-22 can modulate the expression of metabolically relevant hepatocyte genes. However, in diet-induced MASLD, which depends on lipid and sugar absorption in the SI and delivery to the liver via the portal circulation, as well as fructose-induced endotoxemia,[11] the protective effect of IL-22Fc is mediated via IL-22Ra1 signaling in IECs rather than hepatocytes. These findings also apply to STAT3, one of the major conduits through which IL-22 exerts its protective activity. Although hepatocyte-specific STAT3 ablation, previously shown to be needed for IL-22-mediated protection from alcohol-induced liver injury,[16] does not abrogate MASLD resolution by IL-22, its ablation in IECs does block the MASLD protective effect of IL-22. It is also likely that intestinal IL-22 signaling is responsible for the reduction in lethal infections in patients with alcoholic hepatitis.[14]

IL-22 is a unique cytokine produced by Th17/22, γδ T, and ILC3 cells that affects epithelial cells rather than other immune cells.[10] IL-22, along with IL-17A, reduces barrier permeability and maintains microbial homeostasis.[27,37] Although short-term studies have shown that endogenous IL-22 and IL-17A can control occasional and temporary increases in fat or sugar intake,[12,22,23,38] we observed that endogenous IL-22 and IL-22Ra1 did not protect mice from the long-term effects of energy-dense diets, similar to those that drive the obesity and MASLD epidemic. As demonstrated, this is due to the rapid decline in IL-22 expression by ILC3, which is accompanied by a decline in the mRNA amounts of other barrier-protective cytokines; IL-17A, which is mainly expressed in Th17 cells; and IL-23, which is expressed by lamina propria macrophages and DCs. The decline in endogenous *Il22* and *Il17a* mRNAs is paralleled by the marked inhibition of STAT3 phosphorylation in SI IECs of HFD- or WD-fed mice. At this point, it is not clear what happens first—the decline in IL-22 and IL-17A expression or the inhibition of STAT3 activation—but our study shows that exogenous IL-22Fc can restore the expression of endogenous *Il22* and *Il17a* mRNAs and that the effect is STAT3 dependent.

(B) Heatmap of top 25 genes for each cell cluster.
(C) Expression of individual mRNAs in the indicated cell clusters.
(D) Top 20 downregulated Gene Ontology terms (Biological Process) for the Fc- and IL-22Fc-treated cell clusters.
(E) Gene set enrichment analysis (GSEA) focusing on hallmark fatty acid metabolism (left) and transporter (right) genes in the Fc- and IL-22Fc-treated cell clusters.

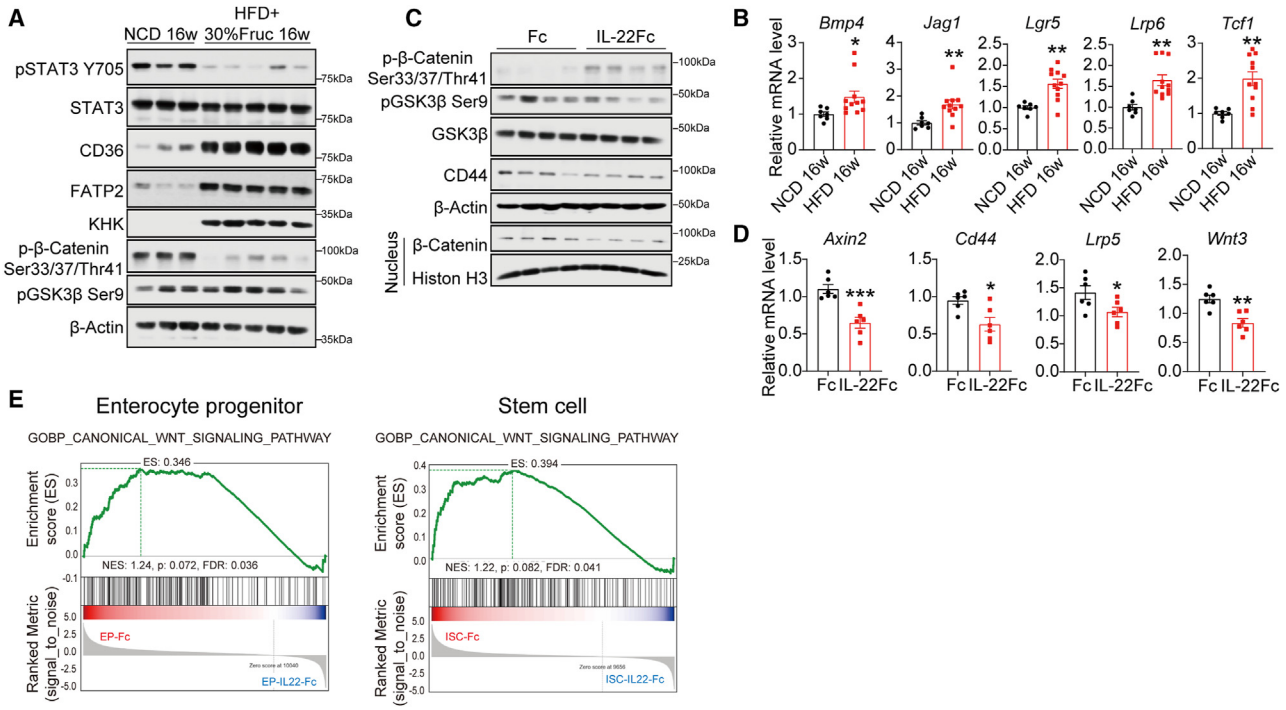

Figure 6. IL-22Fc inhibits Wnt-β-catenin signaling

(A and B) IB (A) and quantitative real-time PCR (B) analyses of indicated SI proteins and mRNAs from C57BL/6 mice kept on NCD (n = 7) or HFD + 30% fructose drink (n = 11) for 16 weeks.

(C and D) Whole-cell and nuclear proteins (C) and mRNA (D) analyses of SI from HFD + fructose-fed C57BL/6 mice treated with Fc (n = 6) or IL-22Fc (n = 6) as above.

(E) GSEA of the indicated cell clusters (from Figure 5) focusing on hallmark Wnt pathway.

Data are presented as mean ± SEM. *p < 0.05, **p < 0.01 (unpaired two-tailed t test).

Moreover, STAT3 ablation in IECs reduced *Il22* mRNA expression, while constitutive activation of STAT3 in the IECs of *gp130*$^{Act\text{-}IEC}$ mice was protective. IL-22Fc administration fully reversed the effects of obesogenic diets on IEC homeostasis, which included expansion of stem cells and mature absorptive enterocytes and induction of lipid[29] and sugar transporters and metabolizing enzymes. IL-22Fc contracted the stem cell and mature enterocyte compartments, expanded transit-amplifying enterocyte progenitors, and decreased the expression of individual lipid and sugar transporters and catabolizing enzymes in all enterocytes. These effects reduced lipid and sugar transport to the liver, with a consequent decrease in hepatic lipid deposition, confirmed by oil red O (ORO) staining and metabolomic analysis. In addition to reducing macronutrient absorption, IL-22Fc blunted barrier permeability and endotoxin translocation. Some of these effects could be related to the marked suppression of IEC KHK expression, which we have shown to account for production of the cytotoxic and barrier-disruptive fructose metabolite fructose-1 phosphate (F1P), which triggers IEC endoplasmic reticulum (ER) stress and downregulates barrier-maintaining TJPs.[11] These effects were STAT3 dependent and correlated with suppression of Wnt-β-catenin signaling, which is important for intestinal homeostasis and expansion of both intestinal stem cells and mature, differentiated enterocytes. In addition to the resolution of hepatosteatosis, the diminished absorption of dietary lipids and sugars reduced liver damage, inflammation, and fibrosis, as well as lipidemia, and inhibited weight gain and even led to weight loss in WD + fructose-fed mice. The induction of weight loss in mice fed obesogenic diets seems to be a direct corollary of the reduced consumption of such diets, which could be due to IL-22-mediated modulation of the appetite controlling peptide YY (PYY).[34] Curiously, the lipid transporters whose expression is suppressed by IL-22Fc and STAT3 are upregulated in CD,[39] a disease that greatly increases MASLD risk.

As mentioned above, ablation of STAT3 in IECs replicated the effects of the obesogenic diets and suppressed *Il22* mRNA expression by ILC3, which was restored by IL-22Fc-induced STAT3 activation. This suggests that the communication between ILC3 and IEC[32] is reciprocal and that IECs are the primary nutrient sensors, although the mechanism by which the HFD or WD inhibits STAT3 activation remains unknown. Restoration of *Il22* mRNA expression correlated with increased *Il23a* mRNA in mucosal macrophages and DCs, but more studies are needed to fully understand how STAT3 in IECs controls IL-22 production by immune cells. Surprisingly, and despite the robust induction of antimicrobial peptides, the effect of IL-22Fc on intestinal microbiota diversity in HFD + fructose-fed mice did not reach statistical significance, although it likely exerted stronger effects on individual bacterial species, whose significance needs to be evaluated. Nonetheless, IL-22Fc continued to activate IEC STAT3 and suppress lipid transporters and sugar catabolizing

CellPress
OPEN ACCESS

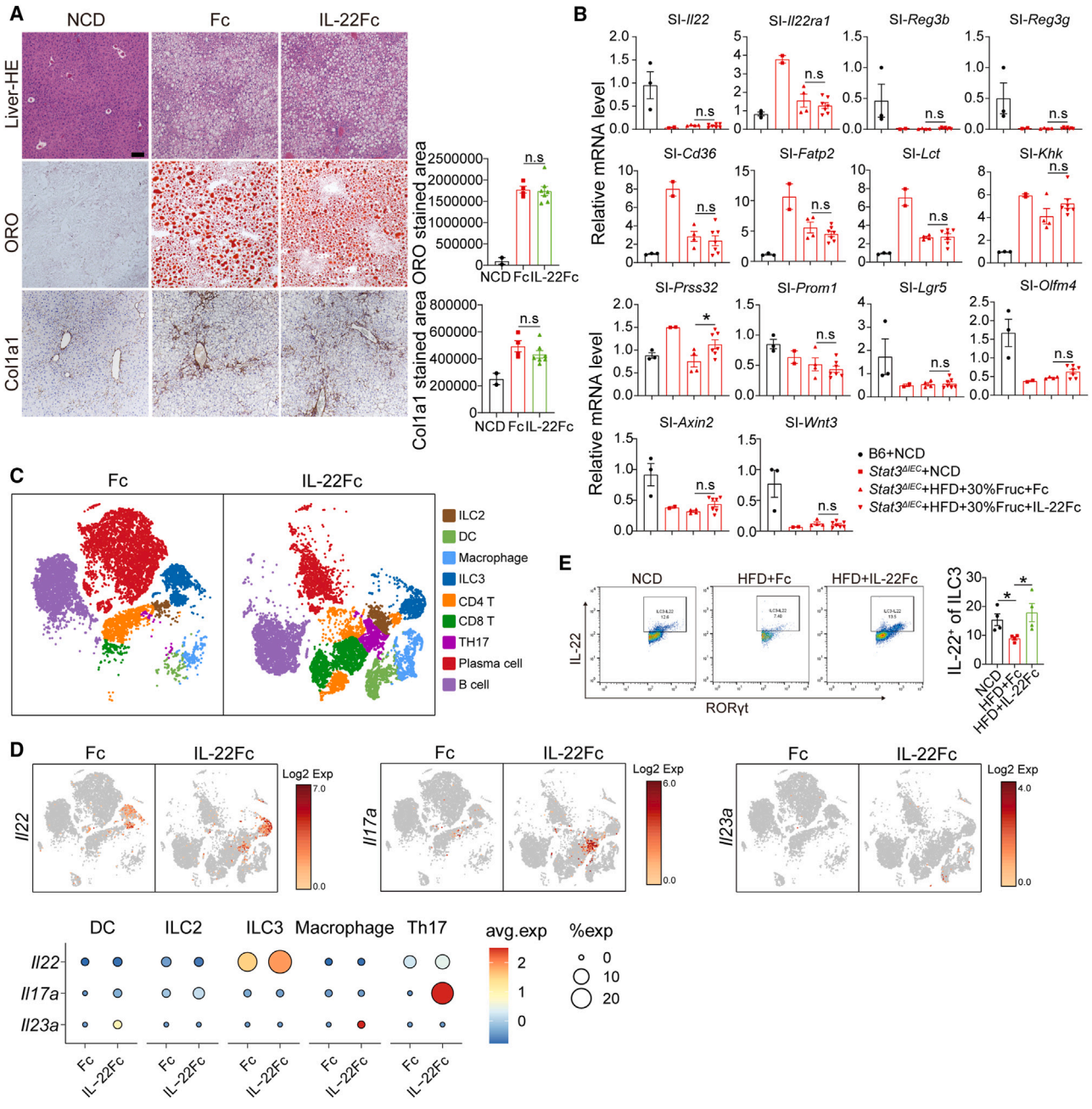

Figure 7. The MASLD remedial effects of IL-22Fc require STAT3 expression in IECs

(A and B) *Stat3*$^{\Delta IEC}$ mice were kept on NCD (n = 2) or HFD + 30% fructose water for 16 weeks and treated with Fc (n = 4) or IL-22Fc (n = 7) as above.

(A) Representative H&E and ORO staining and Col1a1 IHC of liver sections from above mice and quantification. Scale bar, 100 μm.

(B) Quantitative real-time PCR of the indicated SI mRNAs from above mice.

(C and D) SI of C57BL/6 mice fed HFD + fructose and treated with Fc or IL-22Fc was isolated as above and single-cell suspensions of lamina propria lymphocytes were subjected to RNA-seq.

(C) t-SNE plots depicting color-coded clustering of 12,862 and 12,360 single CD45$^+$ immune cells from Fc- and IL-22Fc-treated mice, respectively (n = 2 mice per group), based on known marker genes.

(D) Heatmaps and dot plots of *Il22*, *Il17a*, and *Il23a* mRNA amounts in the designated immune cell populations revealed by scRNA-seq.

(E) Flow cytometric analysis of IL-22 expression in ILC3 (CD45$^+$LIN$^-$CD3$^-$TCRb$^-$TCRg$^-$RORgt$^+$) from the SI of C57BL/6 mice treated with NCD (n = 4), HFD + Fc (n = 4), or HFD + IL-22Fc (n = 4).

Data are presented as mean ± SEM. n.s., not significant; *p < 0.05 (unpaired two-tailed t test).

enzymes in Abx-treated mice that lost >90% of their microbiota. Although the ability of IL-22Fc to induce weight loss, reduce food consumption, and restore liver health was demonstrated in mice, future efforts should focus on development of IEC-selective IL-22R1 agonists, which may be as effective as GLP1 receptor agonists in the treatment of obesity and MASLD, as well as reducing liver fibrosis.

Limitations of the study

Our study, which was conducted in mice, indicates that exogenous IL-22 reverses diet-induced MASLD by binding to its intestinal receptor to inhibit macronutrient absorption through a STAT3-dependent and microbiome-independent signaling. However, how energy-dense diets inhibit IL-22 (and IL-17A) production and how STAT3 in IECs controls IL-22 production by immune cells have not been investigated. Due to the absence of human clinical specimens and suitable publicly available datasets, we could not demonstrate that consumption of obesogenic diets also reduces IL-22 (and IL-17A) production in the human SI. It also needs to be established that IL-22 administration results in MASLD resolution and reversal of dietary obesity in humans. Such conclusions await the completion of ongoing clinical trials.

RESOURCE AVAILABILITY

Lead contact

Further information and requests for resources and reagents should be directed to and will be fulfilled by the lead contact, Michael Karin (karinoffice@ucsd.edu).

Materials availability

All unique/stable reagents generated in this study are available from the lead contact without restriction.

Data and code availability

- 16S rDNA-seq data are available at GEO: GSE242929. scRNA-seq data are available at GEO: GSE242927. Public scRNA-seq data were obtained from a published GEO dataset, GEO: GSE199776. Liver metabolomics data are available at the MassIVE repository (https://massive.ucsd.edu/ProteoSAFe/static/massive.jsp) (MassIVE: MSV000094925).
- All data reported in this paper will be shared by the lead contact upon request. Uncropped western blots and source data related to Figures 1, 2, 3, 4, 5, 6, 7, and S1–S7 can be found in Data S1.
- This paper does not report original code.
- Any additional information required to reanalyze the data reported in this paper is available from the lead contact upon request.

ACKNOWLEDGMENTS

We thank members of the M.K. laboratory for discussions; Cell Signaling Technologies, Santa Cruz Technologies, and MedChemExpress for gifts of antibodies and reagents; UCSD Tissue Technology Shared Resources (TTSR) for histology services; and the San Diego Digestive Diseases Research Center (SDDRC) for 16S (V4) DNA sequencing. Research was supported by grants from the NIH (R37AI043477 and R01DK133448 to M.K.; DK120515 to the SDDRC), Janssen Research & Development, the National Cancer Institute Cancer Center Support Grant (CCSG) (P30CA23100 to TTSR), and the UCSD School of Medicine Microscopy Core (NINDS P30-NS047101). This publication includes data generated at the UCSD IGM Genomics Center utilizing an Illumina NovaSeq 6000 that was purchased with funding from a National Institutes of Health SIG grant (#S10 OD026929).

AUTHOR CONTRIBUTIONS

M.K., P.Z., and J.L. conceived the project. P.Z. and J.L. designed the study and performed most experiments. A.L., I.T., V.D., N.V., H.S., J.Y.K., L.G., M.Z., and S.S. assisted with experiments and data analysis. P.Z. and K.W. performed flow cytometric analysis. M.H. performed NASH CRN scoring. G.B. and J.M.O. performed the MLS assays. S.Z., C.L., and B.S. performed 16S DNA-seq analysis. P.Z. and M.O. performed scRNA-seq and analysis. H.N.Z., S.L., S.M., and P.C.D. performed liver metabolomics and analysis. P.S. provided important reagents and advice and helped with data interpretation and discussion. M.K. and P.Z. wrote the manuscript, with all authors contributing and providing feedback and advice.

DECLARATION OF INTERESTS

M.K. was a founder and stockholder in Elgia Pharmaceuticals and had received research support from Merck and Janssen Pharmaceuticals. P.C.D. consulted for DSM animal health in 2023; is an advisor and holds equity in Cybele, bileOmix, and Sirenas; and is a scientific co-founder and advisor and holds equity in Ometa, Enveda, and Arome, with prior approval by UC San Diego.

STAR★METHODS

Detailed methods are provided in the online version of this paper and include the following:

- KEY RESOURCES TABLE
- EXPERIMENTAL MODEL AND STUDY PARTICIPANT DETAILS
  - Mice
- METHOD DETAILS
  - Olive oil and lactose absorption
  - Measurements of metabolites and hormones
  - GTT and ITT
  - Measurement of intestinal permeability
  - Primary mouse hepatocyte isolation and culture
  - Multi-lineage spheroids (MLS) assay
  - Immunoblot analysis and nuclear extraction
  - Histology
  - RNA isolation and quantitative real-time PCR (qRT-PCR)
  - Liver metabolomics
  - 16s sequencing
  - Isolation of SI epithelial cells and lamina propria lymphocytes
  - Flow cytometry
  - Single-cell RNA sequencing pipeline and analysis
- QUANTIFICATION AND STATISTICAL ANALYSIS

SUPPLEMENTAL INFORMATION

Supplemental information can be found online at https://doi.org/10.1016/j.cmet.2024.08.012.

Received: September 30, 2023
Revised: June 9, 2024
Accepted: August 27, 2024
Published: September 23, 2024

REFERENCES

1. Younossi, Z.M., Koenig, A.B., Abdelatif, D., Fazel, Y., Henry, L., and Wymer, M. (2016). Global epidemiology of nonalcoholic fatty liver disease-Meta-analytic assessment of prevalence, incidence, and outcomes. Hepatology *64*, 73–84. https://doi.org/10.1002/hep.28431.
2. Dufour, J.F., Anstee, Q.M., Bugianesi, E., Harrison, S., Loomba, R., Paradis, V., Tilg, H., Wong, V.W.S., and Zelber-Sagi, S. (2022). Current therapies and new developments in NASH. Gut *71*, 2123–2134. https://doi.org/10.1136/gutjnl-2021-326874.

3. Tilg, H., and Moschen, A.R. (2010). Evolution of inflammation in nonalcoholic fatty liver disease: the multiple parallel hits hypothesis. Hepatology *52*, 1836–1846. https://doi.org/10.1002/hep.24001.

4. Kodali, A., Okoye, C., Klein, D., Mohamoud, I., Olanisa, O.O., Parab, P., Chaudhary, P., Mukhtar, S., Moradi, A., and Hamid, P. (2023). Crohn's disease is a greater risk factor for nonalcoholic fatty liver disease compared to ulcerative colitis: A systematic review. Cureus *15*, e42995. https://doi.org/10.7759/cureus.42995.

5. Kirpich, I.A., Marsano, L.S., and McClain, C.J. (2015). Gut-liver axis, nutrition, and non-alcoholic fatty liver disease. Clin. Biochem. *48*, 923–930. https://doi.org/10.1016/j.clinbiochem.2015.06.023.

6. Febbraio, M.A., and Karin, M. (2021). "Sweet death": fructose as a metabolic toxin that targets the gut-liver axis. Cell Metab. *33*, 2316–2328. https://doi.org/10.1016/j.cmet.2021.09.004.

7. Harrison, S.A., Bedossa, P., Guy, C.D., Schattenberg, J.M., Loomba, R., Taub, R., Labriola, D., Moussa, S.E., Neff, G.W., Rinella, M.E., et al. (2024). A Phase 3, randomized, controlled trial of resmetirom in NASH with liver fibrosis. N. Engl. J. Med. *390*, 497–509. https://doi.org/10.1056/NEJMoa2309000.

8. Mantovani, A., Petracca, G., Beatrice, G., Csermely, A., Lonardo, A., and Targher, G. (2021). Glucagon-like peptide-1 receptor agonists for treatment of nonalcoholic fatty liver disease and nonalcoholic steatohepatitis: an updated meta-analysis of randomized controlled trials. Metabolites *11*, 73. https://doi.org/10.3390/metabo11020073.

9. Newsome, P.N., Buchholtz, K., Cusi, K., Linder, M., Okanoue, T., Ratziu, V., Sanyal, A.J., Sejling, A.S., and Harrison, S.A.; NN9931-4296 Investigators (2021). A placebo-controlled trial of subcutaneous semaglutide in nonalcoholic steatohepatitis. N. Engl. J. Med. *384*, 1113–1124. https://doi.org/10.1056/NEJMoa2028395.

10. Dudakov, J.A., Hanash, A.M., and van den Brink, M.R.M. (2015). Interleukin-22: immunobiology and pathology. Annu. Rev. Immunol. *33*, 747–785. https://doi.org/10.1146/annurev-immunol-032414-112123.

11. Todoric, J., Di Caro, G., Reibe, S., Henstridge, D.C., Green, C.R., Vrbanac, A., Ceteci, F., Conche, C., McNulty, R., Shalapour, S., et al. (2020). Fructose stimulated de novo lipogenesis is promoted by inflammation. Nat. Metab. *2*, 1034–1045. https://doi.org/10.1038/s42255-020-0261-2.

12. Mao, K., Baptista, A.P., Tamoutounour, S., Zhuang, L., Bouladoux, N., Martins, A.J., Huang, Y., Gerner, M.Y., Belkaid, Y., and Germain, R.N. (2018). Innate and adaptive lymphocytes sequentially shape the gut microbiota and lipid metabolism. Nature *554*, 255–259. https://doi.org/10.1038/nature25437.

13. Zai, W., Chen, W., Liu, H., and Ju, D. (2021). Therapeutic opportunities of IL-22 in non-alcoholic fatty liver disease: from molecular mechanisms to clinical applications. Biomedicines *9*, 1912. https://doi.org/10.3390/biomedicines9121912.

14. Arab, J.P., Sehrawat, T.S., Simonetto, D.A., Verma, V.K., Feng, D., Tang, T., Dreyer, K., Yan, X., Daley, W.L., Sanyal, A., et al. (2020). An open-label, dose-escalation study to assess the safety and efficacy of IL-22 agonist F-652 in patients with alcohol-associated hepatitis. Hepatology *72*, 441–453. https://doi.org/10.1002/hep.31046.

15. Radaeva, S., Sun, R., Pan, H.N., Hong, F., and Gao, B. (2004). Interleukin 22 (IL-22) plays a protective role in T cell-mediated murine hepatitis: IL-22 is a survival factor for hepatocytes via STAT3 activation. Hepatology *39*, 1332–1342. https://doi.org/10.1002/hep.20184.

16. Ki, S.H., Park, O., Zheng, M., Morales-Ibanez, O., Kolls, J.K., Bataller, R., and Gao, B. (2010). Interleukin-22 treatment ameliorates alcoholic liver injury in a murine model of chronic-binge ethanol feeding: role of signal transducer and activator of transcription 3. Hepatology *52*, 1291–1300. https://doi.org/10.1002/hep.23837.

17. Yang, L., Zhang, Y., Wang, L., Fan, F., Zhu, L., Li, Z., Ruan, X., Huang, H., Wang, Z., Huang, Z., et al. (2010). Amelioration of high fat diet induced liver lipogenesis and hepatic steatosis by interleukin-22. J. Hepatol. *53*, 339–347. https://doi.org/10.1016/j.jhep.2010.03.004.

18. Gaffen, S.L., Jain, R., Garg, A.V., and Cua, D.J. (2014). The IL-23-IL-17 immune axis: from mechanisms to therapeutic testing. Nat. Rev. Immunol. *14*, 585–600. https://doi.org/10.1038/nri3707.

19. Zheng, M., Horne, W., McAleer, J.P., Pociask, D., Eddens, T., Good, M., Gao, B., and Kolls, J.K. (2016). Therapeutic role of interleukin 22 in experimental intra-abdominal Klebsiella pneumoniae infection in mice. Infect. Immun. *84*, 782–789. https://doi.org/10.1128/IAI.01268-15.

20. Park, O., Ki, S.H., Xu, M., Wang, H., Feng, D., Tam, J., Osei-Hyiaman, D., Kunos, G., and Gao, B. (2015). Biologically active, high levels of interleukin-22 inhibit hepatic gluconeogenesis but do not affect obesity and its metabolic consequences. Cell Biosci. *5*, 25. https://doi.org/10.1186/s13578-015-0015-0.

21. Gao, H., Jin, Z., Bandyopadhyay, G., Cunha, E.R.K., Liu, X., Zhao, H., Zhang, D., Jouihan, H., Pourshahian, S., Kisseleva, T., et al. (2022). MiR-690 treatment causes decreased fibrosis and steatosis and restores specific Kupffer cell functions in NASH. Cell Metab. *34*, 978–990.e4. https://doi.org/10.1016/j.cmet.2022.05.008.

22. Talbot, J., Hahn, P., Kroehling, L., Nguyen, H., Li, D., and Littman, D.R. (2020). Feeding-dependent VIP neuron-ILC3 circuit regulates the intestinal barrier. Nature *579*, 575–580. https://doi.org/10.1038/s41586-020-2039-9.

23. Sullivan, Z.A., Khoury-Hanold, W., Lim, J., Smillie, C., Biton, M., Reis, B.S., Zwick, R.K., Pope, S.D., Israni-Winger, K., Parsa, R., et al. (2021). gamma-delta T cells regulate the intestinal response to nutrient sensing. Science *371*, eaba8310. https://doi.org/10.1126/science.aba8310.

24. Papadopoulos, C., Tentes, I., Papazoglou, D., and Anagnostopoulos, K. (2022). Lysophospholipid metabolism and signalling in non-alcoholic fatty liver disease. Folia Med. (Plovdiv) *64*, 7–12. https://doi.org/10.3897/folmed.64.e59297.

25. Bawa, F.N.C., and Zhang, Y. (2023). Retinoic acid signaling in fatty liver disease. Liver Res. *7*, 189–195. https://doi.org/10.1016/j.livres.2023.07.002.

26. Melis, M., Tang, X.H., Trasino, S.E., and Gudas, L.J. (2022). Retinoids in the pathogenesis and treatment of liver diseases. Nutrients *14*, 1456. https://doi.org/10.3390/nu14071456.

27. Keir, M., Yi, Y., Lu, T., and Ghilardi, N. (2020). The role of IL-22 in intestinal health and disease. J. Exp. Med. *217*, e20192195. https://doi.org/10.1084/jem.20192195.

28. Sabihi, M., Böttcher, M., Pelczar, P., and Huber, S. (2020). Microbiota-dependent effects of IL-22. Cells *9*, 2205. https://doi.org/10.3390/cells9102205.

29. Enriquez, J.R., McCauley, H.A., Zhang, K.X., Sanchez, J.G., Kalin, G.T., Lang, R.A., and Wells, J.M. (2022). A dietary change to a high-fat diet initiates a rapid adaptation of the intestine. Cell Rep. *41*, 111641. https://doi.org/10.1016/j.celrep.2022.111641.

30. Beyaz, S., Mana, M.D., Roper, J., Kedrin, D., Saadatpour, A., Hong, S.J., Bauer-Rowe, K.E., Xifaras, M.E., Akkad, A., Arias, E., et al. (2016). High-fat diet enhances stemness and tumorigenicity of intestinal progenitors. Nature *531*, 53–58. https://doi.org/10.1038/nature17173.

31. Grivennikov, S., Karin, E., Terzic, J., Mucida, D., Yu, G.Y., Vallabhapurapu, S., Scheller, J., Rose-John, S., Cheroutre, H., Eckmann, L., et al. (2009). IL-6 and Stat3 are required for survival of intestinal epithelial cells and development of colitis-associated cancer. Cancer Cell *15*, 103–113. https://doi.org/10.1016/j.ccr.2009.01.001.

32. Diefenbach, A., Gnafakis, S., and Shomrat, O. (2020). Innate lymphoid cell-epithelial cell modules sustain intestinal homeostasis. Immunity *52*, 452–463. https://doi.org/10.1016/j.immuni.2020.02.016.

33. Taniguchi, K., Wu, L.W., Grivennikov, S.I., de Jong, P.R., Lian, I., Yu, F.X., Wang, K., Ho, S.B., Boland, B.S., Chang, J.T., et al. (2015). A gp130-Src-YAP module links inflammation to epithelial regeneration. Nature *519*, 57–62. https://doi.org/10.1038/nature14228.

34. Wang, X., Ota, N., Manzanillo, P., Kates, L., Zavala-Solorio, J., Eidenschenk, C., Zhang, J., Lesch, J., Lee, W.P., Ross, J., et al. (2014). Interleukin-22 alleviates metabolic disorders and restores mucosal

immunity in diabetes. Nature *514*, 237–241. https://doi.org/10.1038/nature13564.

35. Tilg, H., Adolph, T.E., and Trauner, M. (2022). Gut-liver axis: pathophysiological concepts and clinical implications. Cell Metab. *34*, 1700–1718. https://doi.org/10.1016/j.cmet.2022.09.017.
36. Solinas, G., Borén, J., and Dulloo, A.G. (2015). De novo lipogenesis in metabolic homeostasis: more friend than foe? Mol. Metab. *4*, 367–377. https://doi.org/10.1016/j.molmet.2015.03.004.
37. Lee, J.S., Tato, C.M., Joyce-Shaikh, B., Gulen, M.F., Cayatte, C., Chen, Y., Blumenschein, W.M., Judo, M., Ayanoglu, G., McClanahan, T.K., et al. (2015). Interleukin-23-independent IL-17 production regulates intestinal epithelial permeability. Immunity *43*, 727–738. https://doi.org/10.1016/j.immuni.2015.09.003.
38. Kawano, Y., Edwards, M., Huang, Y., Bilate, A.M., Araujo, L.P., Tanoue, T., Atarashi, K., Ladinsky, M.S., Reiner, S.L., Wang, H.H., et al. (2022). Microbiota imbalance induced by dietary sugar disrupts immune-mediated protection from metabolic syndrome. Cell *185*, 3501–3519.e20. https://doi.org/10.1016/j.cell.2022.08.005.
39. Kong, L., Pokatayev, V., Lefkovith, A., Carter, G.T., Creasey, E.A., Krishna, C., Subramanian, S., Kochar, B., Ashenberg, O., Lau, H., et al. (2023). The landscape of immune dysregulation in Crohn's disease revealed through single-cell transcriptomic profiling in the ileum and colon. Immunity *56*, 444–458.e5. https://doi.org/10.1016/j.immuni.2023.01.002.
40. Moh, A., Iwamoto, Y., Chai, G.X., Zhang, S.S.M., Kano, A., Yang, D.D., Zhang, W., Wang, J., Jacoby, J.J., Gao, B., et al. (2007). Role of STAT3 in liver regeneration: survival, DNA synthesis, inflammatory reaction and liver mass recovery. Lab. Invest. *87*, 1018–1028. https://doi.org/10.1038/labinvest.3700630.
41. He, F., Antonucci, L., Yamachika, S., Zhang, Z., Taniguchi, K., Umemura, A., Hatzivassiliou, G., Roose-Girma, M., Reina-Campos, M., Duran, A., et al. (2020). NRF2 activates growth factor genes and downstream AKT signaling to induce mouse and human hepatomegaly. J. Hepatol. *72*, 1182–1195. https://doi.org/10.1016/j.jhep.2020.01.023.
42. Marotz, C., Belda-Ferre, P., Ali, F., Das, P., Huang, S., Cantrell, K., Jiang, L., Martino, C., Diner, R.E., Rahman, G., et al. (2021). SARS-CoV-2 detection status associates with bacterial community composition in patients and the hospital environment. Microbiome *9*, 132. https://doi.org/10.1186/s40168-021-01083-0.
43. Thompson, L.R., Sanders, J.G., McDonald, D., Amir, A., Ladau, J., Locey, K.J., Prill, R.J., Tripathi, A., Gibbons, S.M., Ackermann, G., et al. (2017). A communal catalogue reveals Earth's multiscale microbial diversity. Nature *551*, 457–463. https://doi.org/10.1038/nature24621.
44. Caporaso, J.G., Lauber, C.L., Walters, W.A., Berg-Lyons, D., Huntley, J., Fierer, N., Owens, S.M., Betley, J., Fraser, L., Bauer, M., et al. (2012). Ultra-high-throughput microbial community analysis on the Illumina HiSeq and MiSeq platforms. ISME J. *6*, 1621–1624. https://doi.org/10.1038/ismej.2012.8.
45. Walters, W., Hyde, E.R., Berg-Lyons, D., Ackermann, G., Humphrey, G., Parada, A., Gilbert, J.A., Jansson, J.K., Caporaso, J.G., Fuhrman, J.A., et al. (2016). Improved bacterial 16S rRNA gene (V4 and V4-5) and fungal internal transcribed spacer marker gene primers for microbial community surveys. mSystems *1*, 1. https://doi.org/10.1128/mSystems.00009-15.
46. Marotz, C., Sharma, A., Humphrey, G., Gottel, N., Daum, C., Gilbert, J.A., Eloe-Fadrosh, E., and Knight, R. (2019). Triplicate PCR reactions for 16S rRNA gene amplicon sequencing are unnecessary. BioTechniques *67*, 29–32. https://doi.org/10.2144/btn-2018-0192.
47. Haber, A.L., Biton, M., Rogel, N., Herbst, R.H., Shekhar, K., Smillie, C., Burgin, G., Delorey, T.M., Howitt, M.R., Katz, Y., et al. (2017). A single-cell survey of the small intestinal epithelium. Nature *551*, 333–339. https://doi.org/10.1038/nature24489.
48. Kim, E., Tran, M., Sun, Y., and Huh, J.R. (2022). Isolation and analyses of lamina propria lymphocytes from mouse intestines. Star Protoc. *3*, 101366. https://doi.org/10.1016/j.xpro.2022.101366.
49. Huang da, W., Sherman, B.T., and Lempicki, R.A. (2009). Systematic and integrative analysis of large gene lists using David bioinformatics resources. Nat. Protoc. *4*, 44–57. https://doi.org/10.1038/nprot.2008.211.

STAR★METHODS

KEY RESOURCES TABLE

REAGENT or RESOURCE	SOURCE	IDENTIFIER
Antibodies		
anti-COL1A1	Cell Signaling	Cat# 72026; RRID: AB_2904565
anti-a-SMA	Cell Signaling	Cat# 19245; RRID: AB_2734735
anti-F4/80	Invitrogen	Cat# MF480000; RRID: AB_10376289
anti-p-Stat3 Y705	Cell Signaling	Cat# 9145; RRID: AB_2491009
anti-Stat3	Cell Signaling	Cat# 12640; RRID: AB_2629499
anti-CD36	R&D	Cat# AF2519; RRID: AB_2228767
anti-FATP2	Santa Cruz	sc-393906
anti-KHK	Santa Cruz	sc-377411
anti-β-actin	Sigma	Cat# A4700; RRID: AB_476730
anti-p-β-catenin Ser33/37/Thr41	Cell Signaling	Cat# 9561; RRID: AB_331729
anti-p-GSK3β Ser9	Cell Signaling	Cat# 9323; RRID: AB_2115201
anti-GSK3β	Cell Signaling	Cat# 12456; RRID: AB_2636978
anti-CD44	Bio-Rad	Cat# MCA1967; RRID: AB_323213
anti-β-catenin	Santa Cruz	Cat# sc-1496; RRID: AB_1563968
anti-Histon H3	Abclonal	Cat# A2348; RRID: AB_2631273
anti-Sis	Santa Cruz	Cat# sc-393470; RRID: AB_2630348
anti-Sox9	Abcam	Cat# ab185966; RRID: AB_2728660
anti-Ki67	GeneTex	Cat# GTX16667; RRID: AB_422351
anti-TCR beta- FITC	eBioscience	Cat# 11-5961-85; RRID: AB_465324
anti-TCR gamma/delta-APC	eBioscience	Cat# 17-5711-82; RRID: AB_842756
anti-ROR gamma (t)-PE	eBioscience	Cat# 12-6988-82; RRID: AB_1834470
anti-IL-22-PerCP-eFluor 710	eBioscience	Cat# 46-7221-82; RRID: AB_10598646
anti-CD3- APC/Cyanine7	BioLegend	Cat# 100222; RRID: AB_2057374
anti-IL-17-PECy7	ebioscience	Cat# 25-7177-82; RRID: AB_10732356
anti-CD11b- eFluor 450	eBioscience	Cat# 48-0112-80; RRID: AB_1582237
anti-CD8A eFluor450	eBioscience	Cat# 48-0081-80; RRID: AB_1272235
anti-CD45 violet 510	Biolegend	Cat# 103137; RRID: AB_2561392
anti-CD19 eFluor 450	eBioscience	Cat# 48-0193-82; RRID: AB_2734905
anti-CD11c eFluor 450	eBioscience	Cat# 48-0114-82; RRID: AB_1548654
anti-CD8b-e450	ebioscience	Cat# 48-0083-82; RRID: AB_11218504
anti-F4/80 FITC	ebioscience	Cat# 11-4801-85; RRID: AB_2637192
anti-CD80: PE	Pharmingen	Cat# 553769; RRID: AB_395039
anti-CD206-PerCP-eFluor 710	eBioscience	Cat# 46-2061-82; RRID: AB_2784688
anti-CD3e: PE-Cy7	eBioscience	Cat# 25-0031-82; RRID: AB_469572
anti-Gr-1-PE-Cy7	eBioscience	Cat# 25-5931-82; RRID: AB_469663
anti-CD19 Pe Cy7	biolegend	Cat# 115520; RRID: AB_313654
anti-Cd11b-eFlour 660	eBioscience	Cat# 50-0112-82; RRID: AB_11218507
HRP anti-rabbit IgG	Cell Signaling	Cat# 7074; RRID: AB_2099233
HRP anti-mouse IgG	Cell Signaling	Cat# 7076; RRID: AB_330924
HRP anti-goat IgG	Santa Cruz	Cat# sc-2354; RRID: AB_628490
Biotin goat anti-mouse IgG	BD Pharmingen	Cat# 553999; RRID: AB_395196
Biotin mouse anti-goat IgG	Santa Cruz	Cat# sc-2489; RRID: AB_628488
Biotin goat anti-rabbit IgG	BD Pharmingen	Cat# 550338; RRID: AB_393618
Biotin goat anti-rat IgG	BD Pharmingen	Cat# 559286; RRID: AB_397214

(*Continued on next page*)

Continued

REAGENT or RESOURCE	SOURCE	IDENTIFIER
HRP streptavidin	BD Pharmingen	Cat# 554066; RRID: AB_2868972
Chemicals, peptides, and recombinant proteins		
High fat diet	Bio-Serv	F3282
Western diet	TestDiet	AIX-76A Western Diet
Normal chow diet	LabDiet	5053
mFc	Chimerigen	CHI-MF-120IG2A-0000
rmIL-22-Fc	Chimerigen	CHI-MF-12022-0000
D-(−)-Fructose	Sigma	47748
Olive oil	Sigma	O1514
α-Lactose monohydrate	Sigma	L3625
Insulin	Sigma	11061-68-0
Percoll	GE healthcare	10226958
Liberase TM Research Grade	Sigma	5401127001
Dnase I	Roche Diagnostics	10104159001
Recombinant Mouse IL-22	R&D	582-ML-010
Hematoxylin	Leica	3801615
Eosin	Leica	3801571
Ampicillin sodium salt	Sigma	A0166
VANCOMYCIN HYDROCHLORIDE	VWR	VWRV0990
NEOMYCIN SULFATE	VWR	VWRV0558
Metronidazole	Spectrum Chemical Manufacturing Corporation	M1284
Fluorescein isothiocyanate–dextran (FD4)	Sigma	FD4-100MG
TrypLE express	Gibco	12604013
Critical commercial assays		
NE-PER Nuclear and Cytoplasmic Extraction Reagent kit	Thermo Fisher	78833
3, 3′-diaminobenzidine (DAB) solution	Vector Laboratories	SK-4100
Triglyceride Colorimetric Assay Kit	Cayman Chemical	#10010303
Cholesterol Fluorometric Assay Kit	Cayman Chemical	#10007640
ALT(GPT) Reagent	Thermo Scientific	TR71121
AST/GOT Reagent	Thermo Scientific	TR70121
Insulin ELISA KIT	Invitrogen	EMMINS
Mouse Lipopolysaccharides (LPS) ELISA Kit	CUSABIO	CSB-E13066m
RNeasy Plus Mini kit	Qiagen	#74134
SuperScript VILO cDNA Synthesis Kit	Thermo Fisher Scientific	11754050
Foxp3 / Transcription Factor Staining Buffer Set	eBioscience	00-5523-00
Cytofix/Cytoperm Fixation/Permeabilization Solution Kit	BD	555028
Cell Stimulation Cocktail	eBioscience	00-4970-93
Dead Cell Removal Kit	Miltenyi Biotec	130-090-101
Deposited data		
16s rDNA seq data	This paper	GEO: GSE242929
scRNA-seq data	This paper	GEO: GSE242927
Public scRNA-seq data	Enriquez et al.[29]	GEO: GSE199776
Metabolomics	This paper	MassIVE: MSV000094925
Data S1. Source data	This paper	N/A

(*Continued on next page*)

Continued

REAGENT or RESOURCE	SOURCE	IDENTIFIER
Experimental models: Organisms/strains		
C57BL/6	Charles River Laboratories	N/A
Il22ra1$^{\Delta Hep}$	Dr. Jay Kolls	N/A
Il22ra1$^{\Delta IEC}$	Dr. Jay Kolls	N/A
Stat3$^{\Delta Hep}$	Dr. David Brenner	N/A
Stat3$^{\Delta IEC}$	Dr. David Brenner	N/A
gp130^{Act}	Our lab	N/A
Oligonucleotides		
See Table S1	This paper	N/A
Software and algorithms		
SoftMax 6.5	Molecular Devices	https://www.moleculardevices.com/
ImageJ	NIH	https://imagej.nih.gov/ij/
Graphpad Prism 7	Graphpad	https://www.graphpad.com/scientificsoftware/prism/
Fiji Image J 1.53q	N/A	https://imagej.net/software/fiji/
FlowJo 10.8.1	BD	https://www.flowjo.com/
QIIME 2 pipeline	QIIME 2 Development Team	https://dev.qiime2.org/latest/
R (v4.0.2)	R Project	https://www.r-project.org/
CellRanger v7.1.0	10X Genomics	https://www.10xgenomics.com/
Loupe Brower 6.5.0	10X Genomics	https://www.10xgenomics.com/
GSEA 4.3.2	Broad Institue	https://www.gsea-msigdb.org/gsea/index.jsp

EXPERIMENTAL MODEL AND STUDY PARTICIPANT DETAILS

Mice

C57BL/6 mice were obtained from Charles River Laboratories. *Il22ra1$^{f/f}$* mice[19] were obtained from Prof. Jay Kolls at Tulane University and crossed with either *Albumin^{Cre}* mice (*Alb^{Cre}/Il22ra1$^{f/f}$*) or *Villin^{Cre}* mice (*Villin^{Cre}/Il22ra1$^{f/f}$*) to ablate IL-22Ra1 in either hepatocytes (*Il22ra1$^{\Delta Hep}$*) or IEC (*Il22ra1$^{\Delta IEC}$*). *Stat3$^{\Delta Hep}$* and *Stat3$^{\Delta IEC}$* mice[40] were received from Prof. David Brenner at UCSD. *gp130^{Act}* mice, generated by the Karin lab, were previously described.[33] Mice were randomly allocated to different experimental groups based on their genotypes. In preliminary experiments we found that separate housing of Fc and IL-22Fc treated mice resulted in more robust differences between the two treatment groups. Only male mice were used and kept in filter-topped cages on autoclaved food and water at constant temperature (23 °C ± 2 °C) and humidity (50%–60%), in a pathogen-free controlled environment with a standard 12-h light–12-h dark cycle. Experiments were performed in accordance with UCSD Institutional Animal Care and Use Committee and NIH guidelines and regulations. Animal protocol S00218 (M.K.) was approved by the UCSD Institutional Animal Care and Use Committee. Male mice (10 weeks-old) were fed NCD, HFD (Bio-Serv, F3282) or WD (TestDiet, AIX-76A Western Diet). Both the HFD and WD were supplemented by 30% fructose water. After 12 weeks, the mice were intraperitoneally (i.p.) injected with 10 μg/mouse mFc (Chimerigen, CHI-MF-120IG2A-0000) or mIL-22-Fc (Chimerigen, CHI-MF-12022-0000) every 3 days for 4 more weeks on the same diet as before the treatment. Body weight and food consumption were monitored weekly throughout the entire 16 weeks period, after which the mice were euthanized for blood and tissue collection. The number of mice per experiment was selected based on power calculations and is indicated in the figure legends.

For antibiotics treatment, male C57BL/6 mice (10 weeks-old) were fed HFD+30% fructose water for 16 weeks and were i.p. injected with 10 μg mFc or IL-22Fc /mouse for the last 4 weeks as above. During the last 5 weeks 9i.e. one week prior to Fc or IL-22Fc treatments), 1 g/L ampicillin (Sigma, A0166), 0.5 g/L vancomycin (VWR, VWRV0990), 1 g/L neomycin sulfate (VWR, VWRV0558), and 1 g/L metronidazole were added into 30% fructose water that was changed every 2 days.

METHOD DETAILS

Olive oil and lactose absorption

For measurement of olive oil absorption, C57BL/6 mice, *Il22ra1$^{f/f}$* or *Il22ra1$^{\Delta IEC}$* were HFD fed for 2 weeks, and during the second week of feeding, the mice were treated with Fc or IL-22Fc (10 μg/dose/3d). After 4h fast, mice were intravenously (i.v.) injected with tyloxapol (0.5g/kg) 30 min before intragastrical (i.g.) administration of 15ml/kg olive oil. Then the blood triglycerides concentration from the tail vein was measured from 0 to 6 hours. For measurement of lactose absorption, C57BL/6 mice were treated with Fc or IL-22Fc (10 μg/dose/3d) for 1 week. After 12h fast, the mice were i.g. administered 400 μl of 20% lactose solution. Blood glucose was measured before injection and every 30 min thereafter, for up to 2 h.

Measurements of metabolites and hormones

Liver TG, serum TG and serum cholesterol were measured with Triglyceride Colorimetric Assay Kit (Cayman Chemical #10010303) and Cholesterol Fluorometric Assay Kit (Cayman Chemical #10007640), respectively, according to manufacturer protocols. ALT and AST assays were performed with ALT(GPT) Reagent (Thermo Scientific, TR71121) and AST/GOT Reagent (Thermo Scientific, TR70121), respectively, according to the manufacturer's protocol. Serum LPS and insulin were measured with Mouse Lipopolysaccharides (LPS) ELISA Kit (CUSABIO, CSB-E13066m) and Insulin ELISA KIT (Invitrogen, EMMINS), respectively, according to the manufacturer's protocol.

GTT and ITT

For GTT, B6 mice that were fed WD for 16 weeks with Fc or IL-22Fc treatments for the last 4 weeks, were fasted for 12-14 h and then given 1 g/kg glucose by i.p. injection. Blood glucose was measured before the injection and every 30 min thereafter with a glucometer (OneTouch Ultra 2, One Touch) on blood from superficial tail incision. For ITT, B6 mice that were fed and treated as above, were fasted for 2-4 h and then injected with 0.5 U/kg insulin. Blood glucose was measured before injection and every 30 min thereafter, up to 2 h.

Measurement of intestinal permeability

C57B6 mice were fed with NCD or HFD+30% fructose water for 16 weeks and treated with Fc or IL-22Fc for the last 4 weeks. After a 5 h fast, the mice were gavaged with 50 mg/kg FITC-Dextran (FD4). Serum was collected at 0 and 5 h later and FD4 fluorescence was measured at 530 nm with excitation at 485 nm.

Primary mouse hepatocyte isolation and culture

Primary hepatocytes were isolated from 8 weeks-old *Il22ra1*$^{f/f}$ and *Il22ra1*$^{\Delta Hep}$ males using a two-step collagenase perfusion as described.[41] Briefly, mouse livers were perfused with perfusion buffer (HBSS (Thermo Fisher, 14175095) with 0.5mM EDTA and 25mM HEPES) and digested with digestion buffer (HBSS with Ca^{2+} Mg^{2+} (Thermo Fisher, 24020117), 25mM HEPES and 1mg/ml Liberase (Roche, 5401127001)). Hepatocytes were spun down at 50x g for 3 min at 4 °C then purified on a Percoll gradient. The hepatocytes were counted and directly collected or plated on collagen-coated plates for 6 h in plating medium (DMEM low glucose, 5% FBS and 1% Penicillin-streptomycin (PS)). After cell attachment, the plating medium was replaced with maintenance medium (Williams E medium, 2 mM glutamine and 1% PS) for further use.

Multi-lineage spheroids (MLS) assay

The MLS assay was described previously.[21] Hepatocyte from *Il22ra1*$^{f/f}$ and *Il22ra1*$^{\Delta Hep}$ mice and stellate cell (SC) and non-parenchymal cells (NPCs) from C57BL/6 mice were isolated. Spheroid composition: cells per well of 96-well ultra-low attachment plate Hep:SC:NPC=1600:400:600. Every 3 days, 50% of the medium is replaced by serum free medium. Fibrogenesis was stimulated by a NASH medium containing fatty acids, fructose and LPS. Spheroids were treated with 100ng/ml Fc or rIL-22 for 48 h then harvested for qRT-PCR analysis.

Immunoblot analysis and nuclear extraction

Cells were harvested and lysed in RIPA buffer (50 mM Tris-HCl, pH 7.4, 150 mM NaCl, 1% Triton X-100, 1% sodium deoxycholate, 0.1% SDS, 1 mM EDTA) supplemented with complete protease inhibitor cocktail. Livers and SI were homogenized in a Dounce homogenizer (Thomas Scientific, NJ) with 30 strokes in RIPA buffer supplemented with complete protease inhibitor cocktail. The proteins were separated by SDS-PAGE and transferred to polyvinylidene difluoride (PVDF) membranes, blocked in 5% nonfat milk, and incubated with the indicated primary antibodies overnight. Second antibodies were added for another 1 h and detected with Clarity Western ECL Substrate (Biorad). Nuclear extraction was performed with the NE-PER Nuclear and Cytoplasmic Extraction Reagent kit (Thermo Fisher, 78833), following manufacturer's instructions. After extraction, nuclear and cytoplasmic extracts were separated by SDS-PAGE and analyzed by immunoblotting as above.

Histology

SI or liver tissues were dissected and fixed in 4% paraformaldehyde in PBS and embedded in paraffin. 5 μm thick sections were stained with hematoxylin and eosin (H&E) (Leica, 3801615, 3801571). For frozen block preparation, livers were embedded in Tissue-Tek OCT compound (Sakura Finetek), sectioned, and stained with Oil Red O to visualize TG accumulation. For IHC, after xylene de-paraffinization and rehydration through graded ethanol antigen retrieval was performed for 20 min at 100°C with 0.1% sodium citrate buffer (pH 6.0). Following quenching of endogenous peroxidase activity with 3% H_2O_2 and blocking of non-specific binding with 5% bovine serum albumin buffer, sections were incubated overnight at 4°C with the appropriate primary antibodies followed by incubation with 1:500 biotinylated secondary antibodies for 60 min and 1:500 streptavidin-HRP for 60 min. Bound peroxidase was visualized by 1-10 min incubation in a 3, 3′-diaminobenzidine (DAB) solution (Vector Laboratories, SK-4100). Slides were photographed on an upright light/fluorescent Imager A2 microscope with AxioVision Rel. 4.5 software (Zeiss). All liver samples were scored for steatosis, lobular inflammation, hepatocellular ballooning used for calculation of NAS using published NASH CRN criteria.

RNA isolation and quantitative real-time PCR (qRT-PCR)

Total liver or SI RNA was extracted with RNeasy Plus Mini kit (Qiagen #74134) and cDNA was synthesized with SuperScript VILO cDNA Synthesis Kit (Thermo Fisher Scientific, 11754050). mRNA expression was determined by CFX96 thermal cycler (BioRad). Data are presented as arbitrary units. Primers are listed in Table S1.

Liver metabolomics

OPTIMA-grade acetone, chloroform, methanol (MeOH), acetonitrile (ACN), water, and formic acid were purchased from Fisher Scientific (Pittsburgh, PA). 50 mg of liver tissue from NCD or WD+fructose fed mice treated with Fc or IL-22Fc (n=3 for each group) were thawed on ice for 30 min. A precleaned 5 mm stainless steel bead (Qiagen Inc., Valencia, CA) and 0.5 mL MeOH were added to each sample tube. Samples were homogenized on a TissueLyzer (Qiagen Inc., Valencia, CA; 25 Hz, 5 min), then mixed with 0.5 mL chloroform, vortexed for 20 s, and after adding 0.4 mL water, vortexed again for 20 s, and then centrifuged (16 000 rpm, 15 min). The upper aqueous fraction and the bottom chloroform-lipid fraction were collected into 2 mL glass vials and dried on a vacuum concentrator (liquid volume monitored constantly to avoid over-drying and potential chemical loss). The upper layer was redissolved in 0.2 mL ACN/H_2O 50:50 with 100 ug/L sulfadimethoxine-d5. (this layer was not used for data analysis). The lower layer: was redissolved in ACN/IPA/H_2O 65:30:5 with 100 ug/L sulfadimethoxine-d5 and transferred into glass vial inserts. Triplicate method blanks and 8 instrument controls were included. Tissue extracts were injected (5 μL) into a Vanquish ultra-high-performance liquid chromatography (UHPLC) system coupled to a Q Exactive quadrupole orbitrap mass spectrometer (Thermo Fisher Scientific, Waltham, MA). A Kinetex polar C18 column (150 × 2.1 mm2, 2.6 μm particle size, 100 A pore size; Phenomenex, Torrance) was employed with a SecurityGuard C18 column (2.1 mm ID) at 30 °C column temperature. The mobile phases (0.5 mL/min) were 0.1% formic acid in both water (A) and ACN (B) with the following gradient: 0–1 min 5% B, 1–7 min 5–100% B, 7–7.5 min 100% B, 7.5–8 min 100–5% B, and 8–10 min 5% B. The mass spectrometer was operated in positive heated electrospray ionization (see Text S1 for detailed instrumental parameters). The raw spectra were converted to.mzML files using MSconvert (ProteoWizard), followed by feature extraction with MZmine 3.2.8. Peak areas of the chemical features were used for quantification. LC-HRMS data files are available through the MassIVE repository (https://massive.ucsd.edu/ProteoSAFe/static/massive.jsp) under the following identifier: MassIVE MSV000094925.

16s sequencing

Colonic fecal pellets from HFD+fructose fed *Il22ra1*$^{f/f}$, *Il22ra1*$^{\Delta Hep}$, *Il22ra1*$^{\Delta IEC}$ and Abx-treated C57BL/6 mice treated with Fc or IL-22Fc ($n \geq 6$ for each group) were subjected to nucleic acid extraction at the UCSD Microbiome Core according to previously published protocols.[42] Briefly, samples were purified using the MagMAX Microbiome Ultra Nucleic Acid Isolation Kit (Thermo Fisher Scientific, USA) and automated on KingFisher Flex robots (Thermo Fisher Scientific, USA). Blank controls and mock communities (Zymo Research Corporation, USA) were included and carried through all downstream processing steps. 16S rRNA gene amplification was performed according to the Earth Microbiome Project protocol.[43] Briefly, Illumina primers with unique forward primer barcodes[44] were used to amplify the V4 region of the 16S rRNA gene (515fB-806r[45]). Amplification was performed as single reactions per sample,[46] then equal volumes of each amplicon were pooled and the libraries sequenced on the Illumina NovaSeq 6000 sequencing platform with paired-end 150 bp cycles at the Institute for Genomic Medicine (IGM, UC San Diego). Sequence data were analyzed using QIIME 2 pipeline and R.

Isolation of SI epithelial cells and lamina propria lymphocytes

Isolation of single crypts-enriched epithelial cells was adapted from a published publication.[47] In brief, mesenteric fat tissue and Peyer's patches were carefully removed and the SI was opened longitudinally and sliced into small fragments roughly 2 mm in length. The tissue was incubated in 5 mM EDTA–PBS on ice for 90 min. Every 30 min, the tissue was shaken vigorously and the supernatant was collected as fraction 1 in a new conical tube. The final fraction (enriched for crypts) was washed twice in PBS, centrifuged at 300g for 5 min, and dissociated with TrypLE express (Invitrogen) for 5 min at 37 °C. The single-cell suspension was then passed through a 40-μm filter and dead cells were removed using Dead Cell Removal Kit (Miltenyi Biotec, 130-090-101) for scRNA-seq. Isolation of lamina propria lymphocytes (CD45$^+$) also followed a published protocol.[48] After IEC were removed, the remaining tissue was minced with scissors and dissociated in RPMI containing 2% FBS, Liberase (31.25 μg/ml) and DNase I (50 μg/ml; Roche Diagnostics) at constant shaking at 37 °C for 35 min (175 rpm). The digested tissue was then filtered through a 70-μm strainer to remove large debris. Viable lamina propria lymphocytes were collected at the interface of a 40%/80% Percoll/RPMI gradient (GE Healthcare) and dead cells were removed as above.

Flow cytometry

For lymphocyte isolation, liver fragments of equal weight were cut into small pieces and incubated in dissociation solution (DMEM medium supplemented with collagenase type I (1.5 mg/ml) and DNase I (100 μg/ml)) for 30 min at 37 °C. After incubation, cell suspensions were passed through a 40 μm cell strainer and washed twice. Lamina propria lymphocytes from the SI were isolated as described above. To block Fc-mediated interactions, mouse cells were pre-incubated with 0.5–1 μg of purified anti-mouse CD16/CD32 per 100 μl. Isolated cells were stained with labelled antibodies in PBS with 2% FBS and 2 mM EDTA. Dead cells were excluded on the basis of staining with Propidium Iodide (P4864, Sigma-Aldrich). For intracellular cytokine staining, cells were re-stimulated with cell stimulation cocktail (eBioscience; containing PMA and ionomycin), in the presence of a protein transport inhibitor cocktail containing Brefeldin A (BD). After 4–5 h,

cells were fixed and permeabilized eBioscience Foxp3/Transcription Factor staining buffer for combined staining of cytokines with transcription factors. After fixation/permeabilization, cells were stained with labelled antibodies of interest. Cells were analysed on a Beckman Coulter Cyan ADP flow cytometer. Gating strategies: ILC3 (LiveCD45$^+$CD11c$^-$CD19$^-$CD11b$^-$CD3$^-$TCRβ$^-$TCRγ$^-$RORγt$^+$), Th17 cells (LiveCD45$^+$CD11c$^-$CD19$^-$CD11b$^-$CD3$^+$TCRβ$^+$TCRγ$^-$RORγt$^+$), γδ T cells (LiveCD45$^+$CD11c$^-$CD19$^-$CD11b$^-$CD3$^+$TCRβ$^-$TCRγ$^+$RORγt$^+$), Kupffer cells (LiveCD45$^+$CD3$^-$CD19$^-$Ly6G$^-$F4/80$^+$CD11b^{int}), monocytes derived macrophage (LiveCD45$^+$CD3$^-$CD19$^-$Ly6G$^-$F4/80$^-$CD11b^{high}). Data were analyzed using FlowJo 10.2 software (Treestar).

Single-cell RNA sequencing pipeline and analysis

Single cell RNA-Sequencing (scRNA-seq) library preparation was performed by Prof. Judith Varner lab using the 10x 3' Continuous Chromium Connect. Approximately 17,000 cells were loaded to achieve 10,000 captured cells per sample to be sequenced. Sequencing was performed at the UCSD IGM core facility using the NovaSeq 6000 (Illumina) sequencing platform to obtain approximately 200 million reads per sample. Raw scRNA-seq data was converted to FASTQ files and then aligned to the mouse genome [mm10]-2020 A and integrated using default parameters of CellRanger (v7.1.0, 10x Genomics). Quality control and clustering were performed using Loupe Brower 6.5.0. Basic filtering parameters included cells with Unique Molecular Identifiers (UMIs) of minimum 50 and maximum 8500. Cells expressing less than 50 percent mitochondrial related genes were included and CD45$^+$ cells were removed. After clustering, detected clusters were mapped to cell types or intermediate states using known markers for intestinal epithelial cell subtypes. Differentially expressed genes (DEG) per cluster and Violin plots of genes of interested were calculated and prepared by the Loupe Browser.

To perform Gene Ontology-Term analysis based on biological processes using David,[49] we used DEGs as target genes. To perform GSEA analysis, we used GSEA software with gene sets of fatty acid metabolism, fatty acid transport and canonical WNT signaling pathway from Mouse MSigDB v2023.1.Mm. To perform public scRNA-seq analysis, we first downloaded the Fastq files of NC and HFD 7d from GSE199776 and performed scRNA-seq analysis using the same method as above.

QUANTIFICATION AND STATISTICAL ANALYSIS

Positive areas of protein expression in liver and SI was quantified using 'Colour Deconvolution', 'H DAB', and 'Analyze Particles' feature in Fiji Image J and then averaged across all the fields (5–6 fields). These measurements were done on randomly selected fields of view. A two-tailed unpaired Student's t-test was performed for statistical analysis using GraphPad Prism software. Data are presented as mean ± s.e.m. (****$p < 0.0001$, ***$p < 0.001$, **$p < 0.01$ and *$p < 0.05$). All experiments were repeated at least 3 times.